

1 **Integrating suspended sediment flux in large,**
2 **morphologically complex river channels: Application of**
3 **a synoptic Rouse-based model to the Irrawaddy and**
4 **Salween rivers**

5 **J. Jotautas Baronas¹, Emily I. Stevenson¹, Christopher R. Hackney^{2,3},**
6 **Stephen E. Darby⁴, Michael J. Bickle¹, Robert G. Hilton⁵, Christina S.**
7 **Larkin¹, Daniel R. Parsons², Aung Myo Khaing⁶, Edward T. Tipper¹**

8 ¹Dept. of Earth Sciences, University of Cambridge, UK

9 ²Energy and Environmental Institute, University of Hull, UK

10 ³School of Geography, Politics and Sociology, Newcastle University, UK

11 ⁴School of Geography and Environmental Science, University of Southampton, UK

12 ⁵Dept. of Geography, Durham University, UK

13 ⁶Directorate of Water Resources and Improvement of River Systems, Yangon, Myanmar

14 **Key Points:**

- 15 • An updated empirical Rouse modeling framework to calculate sediment flux and
16 composition in large, hydrodynamic rivers.
- 17 • Model applied to compute annual sediment flux of Irrawaddy and Salween rivers
18 as 326^{+91}_{-70} and 159^{+78}_{-51} Mt/yr, respectively.
- 19 • Fluxes calculated using simple means of depth point samples result in errors of
20 up to 50% relative to Rouse-based model.

Corresponding author: J. Jotautas Baronas, jotautas.baronas@gmail.com

21 Abstract

22 A large portion of freshwater and sediment is exported to the ocean by a small number
 23 of major rivers. Many of these mega-rivers are subject to substantial anthropogenic pres-
 24 sures, which are having a major impact on water and sediment delivery to deltaic ecosys-
 25 tems. Due to hydrodynamic sorting, sediment grain size and composition varies strongly
 26 with depth and across the channel in large rivers, complicating flux quantification. To
 27 account for this, we modified a semi-empirical Rouse model, synoptically predicting sed-
 28 iment concentration, grain size distribution, and organic carbon (%OC) composition with
 29 depth and across the river channel. Using suspended sediment depth samples and flow
 30 velocity data, we applied this model to calculate sediment fluxes of the Irrawaddy and
 31 the Salween, the last two free-flowing mega-rivers in Southeast Asia. Deriving sediment-
 32 discharge rating curves, we calculated an annual sediment flux of 326^{+91}_{-70} Mt/yr for the
 33 Irrawaddy and 159^{+78}_{-51} Mt/yr for the Salween, together exporting 46% as much sediment
 34 as the Ganges-Brahmaputra system. The mean flux-weighted sediment exported by the
 35 Irrawaddy is significantly coarser ($D_{84} = 193 \pm 13 \mu m$) and OC-poorer ($0.29 \pm 0.08 wt\%$)
 36 compared to the Salween ($112 \pm 27 \mu m$ and $0.59 \pm 0.16 wt\%$, respectively). Both rivers
 37 export similar amounts of particulate organic carbon, with a total of $1.9^{+1.4}_{-0.9}$ Mt C/yr,
 38 53% as much as the Ganges-Brahmaputra. These results underline the global significance
 39 of the Irrawaddy and Salween rivers and warrant continued monitoring of their sediment
 40 flux, given the increasing anthropogenic pressures on these river basins.

41 1 Introduction

42 Rivers are the main conduits of dissolved and particulate matter from the conti-
 43 nents to the oceans. Accurate quantification of material exported by rivers is thus of-
 44 ten the most reliable and efficient way to constrain such key processes as continental ero-
 45 sion, chemical weathering, and organic carbon cycling (e.g., Meybeck, 1987; Gaillardet
 46 et al., 1999; West et al., 2005; Viers et al., 2013; Galy et al., 2015; Horan et al., 2019),
 47 leading to an improved understanding of the long-term controls on Earth surface con-
 48 ditions (e.g., Mackenzie & Garrels, 1966; France-Lanord & Derry, 1997; Berner & Kothavala,
 49 2001; Godderis et al., 2009; Maher & Chamberlain, 2014; Hilton et al., 2015), as well as
 50 the anthropogenic perturbation of these processes (e.g., Wilkinson & McElroy, 2007; Al-
 51 lison et al., 2007; Syvitski & Kettner, 2011; Best, 2019). On a global scale, the world's
 52 30 largest rivers by discharge are estimated to account for $\sim 50\%$ of all freshwater and

53 ~25% of all particulate matter export to the ocean (Milliman & Farnsworth, 2011). South-
54 east Asian rivers in particular dominate the global sediment flux, delivering about 2/3
55 of the supply to the ocean, due to a combination of active tectonics and monsoonal cli-
56 mate (Milliman & Farnsworth, 2011). The sediment fluxes of the Ganges-Brahmaputra,
57 Mekong, Irrawaddy, and other major Southeast Asian rivers maintain extensive and fer-
58 tile deltas, supporting large natural and agricultural ecosystems – the primary food source
59 for several hundred million people. In addition, the tropical monsoonal climate enables
60 high net primary productivity and efficient export and oceanic burial of biospheric car-
61 bon – an important sink for atmospheric CO₂ (e.g., Galy et al., 2007; Hilton et al., 2008;
62 Galy et al., 2015). Constraining the sediment and particulate organic carbon flux of large
63 Southeast Asian rivers can help significantly reduce uncertainties in the global exogenic
64 carbon cycle, helping both determine the importance of natural feedback processes, as
65 well as the scale of human perturbation in these river basins.

66 Accurately measuring the total sediment flux and its mean physicochemical com-
67 position is difficult in large rivers due to hydrodynamic sorting of sediments, which re-
68 sults in strong gradients in sediment grain size, concentration and mineral composition
69 with depth (Rouse, 1950; Dietrich, 1982; Jordan, 1965). Although turbulent shear forces
70 affect all particles equally, heavier (larger and denser) particles have higher settling ve-
71 locities (Rouse, 1950; Dietrich, 1982). Suspended sediment concentration (SSC) at the
72 surface is therefore not representative of the total sediment flux, which may be assessed
73 by collecting discrete instantaneous samples at different depths, or by collecting a sin-
74 gle depth-integrated sample, where the sampler is filled at a constant rate while being
75 vertically lifted through the water column; however, it is often unclear how representa-
76 tive single depth-integrated samples are, as the quality of integration strongly depends
77 on sampler geometry, the speed at which the sampler is lifted through the water column,
78 and the ability to maintain isokinetic sampling conditions (e.g., Murray Hicks & Gomez,
79 2016). The point-sampling approach has a major advantage, in that it allows an empir-
80 ical calibration of sediment concentration as a function of flow conditions specific to each
81 sample in the river reach of interest, potentially enabling the mapping of sediment load
82 synoptically (with depth and across the river channel).

83 To date, most sediment flux and composition estimates of large rivers still rely on
84 surface samples, with the notable exceptions being the Amazon and its major tributaries
85 (Bouchez, Lupker, et al., 2011), Ganges (Lupker et al., 2011), Changjiang (Guo & He,

2011), Mekong (Darby et al., 2016), Huanghe (Wang et al., 2007), Orinoco (Meade, 1994), and Mississippi (Meade & Stevens, 1990) rivers, which all have estimates derived via depth- and cross-channel sampling. A previously reported Irrawaddy River flux is also based on depth sampling, however, primarily using data collected in the 19th century using techniques which have since been significantly refined (Gordon, 1880; Robinson et al., 2007); see discussion below. All of the above-mentioned point-sampling studies of large rivers have revealed large variations in sediment concentration and composition with depth, indicating the need for depth (and lateral) sampling to obtain accurate estimates of sediment concentration and flux.

With the advent of Acoustic Doppler Current Profiler (ADCP) technology, it is now relatively simple and routine to measure flow velocity distribution in two dimensions (laterally and with depth) with sub-meter resolution in large river channels (e.g., Yorke & Oberg, 2002; Thorne & Hanes, 2002; Parsons et al., 2013). As a result, a number of attempts have been made to obtain a fully parametrized law for hydrodynamic sorting, which would allow the use of flow velocity data to predict sediment distribution across a river channel, with the need of just a few reference point samples. These attempts have revealed that the original Rouse model (Rouse, 1950) is unable to properly parametrize sediment distributions as function of velocity and depth, whether in large rivers (Bouchez, Métivier, et al., 2011; Lupker et al., 2011), or in flume experiments (Muste et al., 2005, and references therein). The possible reasons are the complex distribution of particle sizes and shapes (Lupker et al., 2011), particle aggregation due to organic matter (Bouchez, Métivier, et al., 2011), and the complex variation of the water and sediment diffusivity coefficients with sediment concentration (Muste et al., 2005; Pal & Ghoshal, 2016).

As an alternative, a number of indirect (surrogate) methods to determine riverine suspended loads, relying on optical and acoustic detection of sediments, have been tested (e.g., Gray & Gartner, 2009; Armijos et al., 2017). In particular, ADCP instruments determine water flow velocity by using the acoustic echo from suspended particles, potentially allowing the simultaneous quantification of SSC with depth and across the river channel with high resolution (e.g., Thorne & Hanes, 2002). ADCP backscatter signal was successfully calibrated to calculate sediment flux of the Mekong River (Darby et al., 2016) and more recently, the Paraña River (Szupiany et al., 2019). A number of complications have so far limited the applicability of this approach, however. Firstly, acoustic instruments have variable sensitivity to different particles, most strongly impacted by grain

119 size. Therefore, a single-frequency instrument is often unable to capture SSC variations
120 in large rivers with complex, often multi-modal particle size distributions and/or vari-
121 able hydrodynamic conditions (e.g., Latosinski et al., 2014). Secondly, the calibration
122 is typically instrument-specific such that raw data between two instruments (even of the
123 same model) may not be comparable, requiring individual calibration for each acoustic
124 instrument.

125 As a result, a hybrid empirical-theoretical approach based on the Rouse equation
126 (Rouse, 1950, see Section 3) has emerged as a robust way to quantify suspended sedi-
127 ment flux and chemical composition in large rivers with complex particle size distribu-
128 tions and/or highly variable hydrodynamic conditions (Bouchez, Lupker, et al., 2011; Lup-
129 ker et al., 2011). Instead of attempting to calibrate acoustic or optical sensing instru-
130 ments, or to determine particle settling velocities for a fully theoretical prediction of SSC,
131 point depth samples are collected to empirically calibrate the SSC-depth relationship un-
132 der known hydrodynamic conditions (determined using ADCP). This approach assumes
133 that instantaneous point samples are representative of equilibrium conditions (i.e., there
134 is no net sediment suspension/deposition within the immediate channel reach). Any re-
135 sulting error due to short-term turbulent fluctuations (e.g., Diplas et al., 2008) can be
136 mitigated by collecting and averaging a larger number of samples (keeping in mind lo-
137 gistical constraints). This empirical calibration is repeated under different hydrodynamic
138 conditions, which enables the construction of a SSC-discharge rating curve. Lupker et
139 al. (2011) have demonstrated how point depth-sampling coupled with ADCP velocity
140 measurements can enable more robust estimates of sediment flux, especially in kilometer-
141 scale wide river channels with complex hydrodynamics and large lateral variations in flow
142 velocity and sediment flux.

143 Here, we present an alternative approach to empirically calibrating the Rouse equa-
144 tion describing the SSC vs. depth vs. flow velocity relationship, and apply this frame-
145 work to the Irrawaddy and the Salween rivers in Myanmar. In contrast to previous ef-
146 forts, this method makes fewer averaging assumptions and allows us to synoptically map
147 high-resolution spatial variations in sediment concentration and composition both across
148 the river channel and with depth. We use this approach to provide new estimates of the
149 sediment and particulate organic carbon export flux by the Irrawaddy-Salween river sys-
150 tem and compare them to values obtained using simple averaging approach, as well as
151 previously published estimates.

2 Methods

2.1 Study site

The Irrawaddy (also known as Ayeyarwady) and the Salween (also known as Thanlwein) are believed to be among the largest rivers in terms of water and sediment flux globally, although previous data are scarce (Robinson et al., 2007; Furuichi et al., 2009; Chapman et al., 2015). The headwaters of the Irrawaddy originate in the southern margin of the eastern Himalayan Syntaxis. It runs for about 2000 km, spanning the whole length of Myanmar and forming a large delta distributary network in the south prior to discharging into the Andaman Sea, with a basin surface area (taking topographic roughness into account using a 90m-resolution DEM) of 437,000 km^2 . The Salween originates in the Tibetan Plateau, traverses the Syntaxis, and flows south across the Shan Plateau in southeastern Myanmar. It has a length of around 2800 km and a basin surface area of 283,000 km^2 (Fig. 1a). The Irrawaddy basin has a large central (relatively dry) valley, with a mean and maximum elevation of 862 and 5798 m, respectively, and a median slope of 7.1 degrees. In contrast, the Salween catchment is steep and narrow for such a large basin, with a mean and maximum elevation of 3515 and 6857 m, respectively, and a median slope of 16.4 degrees.

Both river basins are comprised of a wide variety of sedimentary, igneous and metamorphic rocks, ranging from Pre-Cambrian to Cenozoic in age and transposed by a complex network of sutures and faults (e.g., Searle et al., 2007; Mitchell et al., 2012; Licht et al., 2013; Khin Zaw et al., 2017; Zhang et al., 2018; Westerweel et al., 2019; Najman et al., 2020). The climate of both basins is dominated by the southwest Asian monsoon (and to a lesser degree the northeast monsoon), with most precipitation and discharge taking place in June through September (Khin Zaw et al., 2017). Mean annual precipitation rates vary from <800mm/yr up to >4000 mm/yr within the Irrawaddy basin, depending on the location (e.g., Chen et al., 2017; Sein et al., 2018). Most water to both rivers is supplied by the monsoon precipitation, with additional (unquantified, but likely minor and further diminishing) inputs from mountain glacier melt and snowmelt in the north.

In terms of water and sediment flux and their chemical composition, the Irrawaddy and the Salween have very little data available compared to other Asian megarivers, largely due to historically difficult access to the country of Myanmar, which contains the ma-

184 jor portions of both catchments (Fig. 1). The little data that are available point to the
185 Irrawaddy-Salween system being a globally significant source of sediment and POC to
186 the ocean but these estimates have a large uncertainty (Robinson et al., 2007; Bird et
187 al., 2008; Furuichi et al., 2009). The Irrawaddy-Salween have remained largely undammed,
188 with free flowing mainstems (Grill et al., 2019) and only several small dams on minor
189 tributaries, totalling around 2500 MW generation capacity across both basins. However,
190 over 40 dams, ranging from small to very large (>5000 MW) have been announced and
191 are either in planning or construction stage on the two rivers, with a total capacity of
192 more than 45000 MW (Kirchherr et al., 2017; Lazarus et al., 2019), which will signifi-
193 cantly alter their water and sediment discharge dynamics. In addition, Southeast Asian
194 river sand is a major construction resource that is often unsustainably dredged and be-
195 coming increasingly scarce, resulting in bank erosion and collapse downstream and con-
196 demning low-lying river deltas to seawater intrusion and inundation (Xiqing et al., 2006;
197 Kondolf et al., 2018; Best, 2019; Bendixen et al., 2019; Hackney et al., 2020). All together,
198 damming, sand mining, and climate change will likely have a large impact on the Irrawaddy-
199 Salween sediment fluxes, with negative consequences for downstream ecosystems and com-
200 munities. It is therefore crucial to establish a baseline of the current sediment flux and
201 composition, so that any impact from potential future environmental change can be ac-
202 curately assessed.

203 **2.2 Discharge measurements using ADCP**

204 Flow velocity measurements and sediment samples of the Irrawaddy-Salween rivers
205 were collected during two monsoon seasons, in August 2017 and 2018, and two dry sea-
206 sons, in February 2018 and May 2019. Both rivers were sampled just upstream of their
207 delta distributary networks (Fig. 1). Depth profiles of suspended sediments were collected
208 each time, except in February 2018, when only surface samples were collected.

209 Flow velocity was measured using an Acoustic Doppler Current Profiler (ADCP)
210 Rio Grande II (1200 kHz) made by Teledyne Instruments, deployed on a moving boat.
211 The ADCP was attached on a rigid frame close to the bow, in a down-facing orientation,
212 and the transducer submerged at 40-60 cm depth. Data were collected while the boat
213 crossed the river perpendicular to the flow. Boat position during the transect was recorded
214 using an external GPS unit with horizontal accuracy better than 5m. Between 1 and 5
215 such transects were collected, depending on the site, with discharge reproducibility typ-

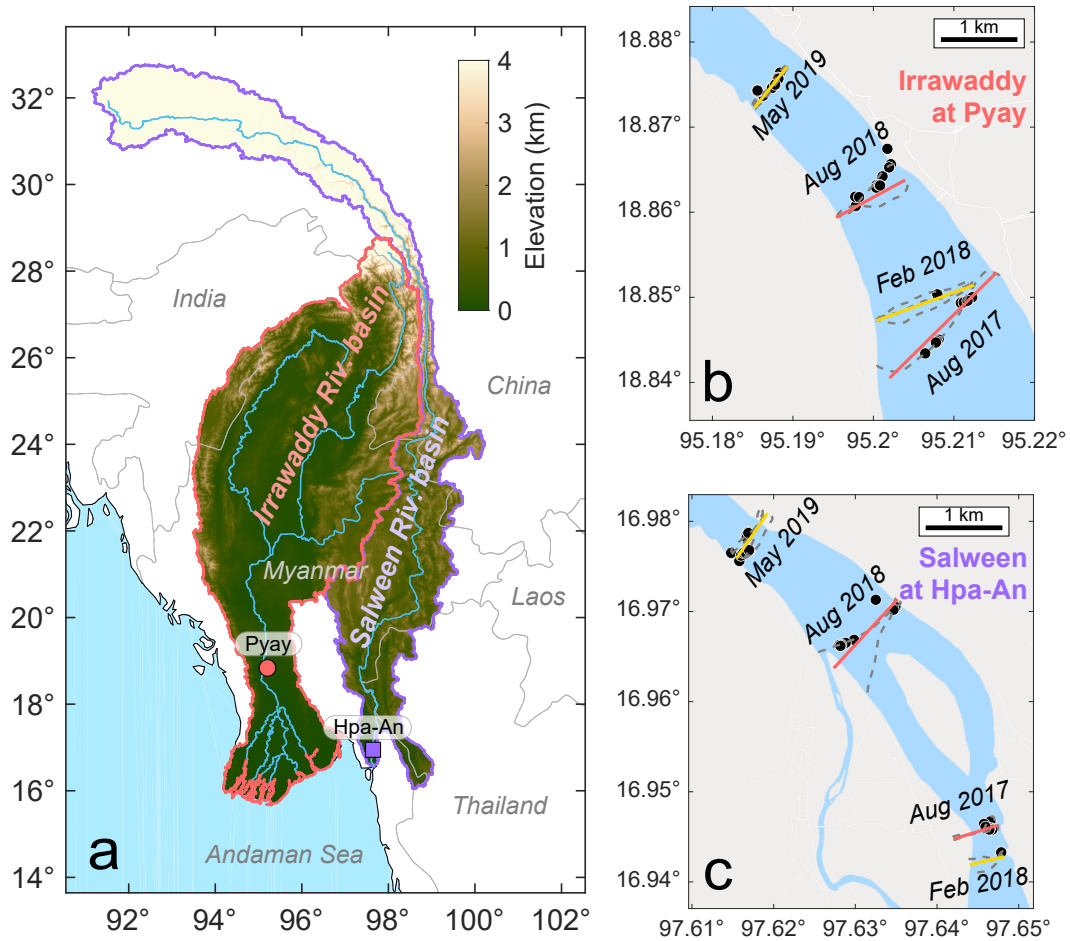


Figure 1. Map indicating the location of the study sites. a) Topographic map of the Irrawaddy and the Salween river basins, outlined in red and purple, respectively; country borders are shown as thin gray lines. The two sampling locations (Pyay on the Irrawaddy and Hpa-An on the Salween) are shown as a circle and a square, respectively. b, c) Detailed view of the ADCP transects (dashed gray lines) and the constructed mean cross sections (solid yellow and red lines) at each sampling location. Sediment depth sample locations are shown as black circles. Note that the exact channel course and width fluctuates seasonally and inter-annually and the channel shown in blue is an approximation.

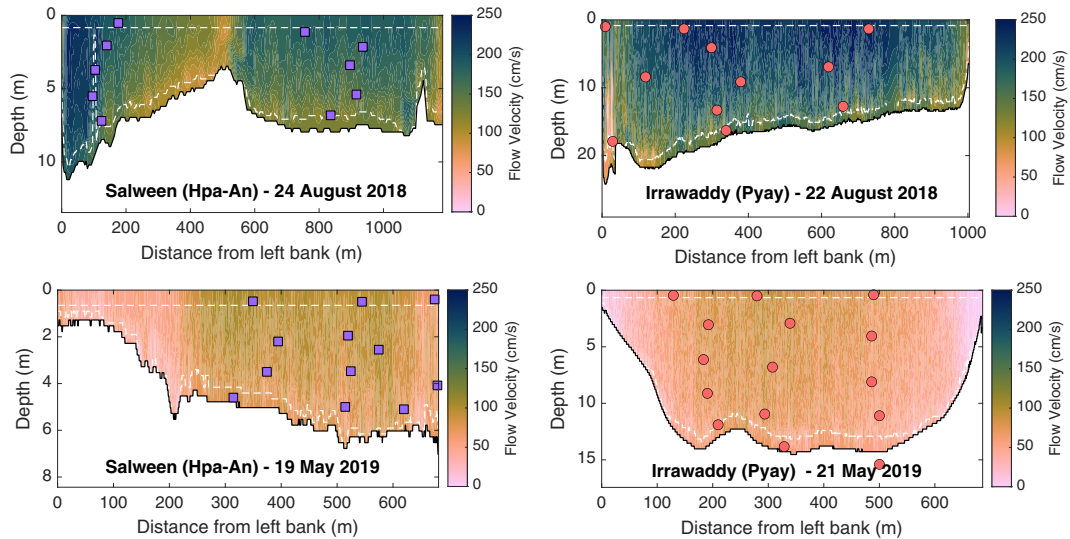


Figure 2. Examples of channel mean cross-sections (MCS) showing the water velocity distribution in the wet and the dry season at each site. Note the differences in axes scales of each panel. The squares and the circles show suspended sediment depth sample locations, projected flow-wise onto the MCS (see Fig. 1b-c for a top-down view of actual sampling locations). The white dashed lines show the regions where flow velocity data were extrapolated at the top (above ADCP transducer depth and blanking distance) and the bottom (below sidelobe interference) of each cross-section (see Section 2.2).

216 ically better than 6%, in agreement with previous applications of moving-vessel ADCP
 217 (e.g., Szupiany et al., 2007).

218 ADCP data were collected and initially processed using WinRiver II software. The
 219 data were then exported and further processed using Velocity Mapping Toolbox (Parsons
 220 et al., 2013). Using multiple river cross-sectional transects, a mean cross-section (MCS)
 221 was created for each sampling date (Fig. 2), ensuring it was perpendicular to river chan-
 222 nel, and calculating the average stream-wise flow velocity field across the river channel
 223 (Fig. 1b,c). The data were then additionally processed in MATLAB 2019b, interpolat-
 224 ing data gaps and removing erroneous outlier data (e.g., due to excessive pitch and roll)
 225 and extrapolating to the river surface (above ADCP transducer) and bottom (below side-
 226 lobe interference) using *inpaint_nans* function (D’Errico, 2018).

2.3 Sediment sample collection and processing

Sediment samples were collected at various depths using a modified 8.5L capacity Van Dorn depth sampler (a Perspex acrylic tube open at both ends, with pneumatically triggered doors, modified from Wildco, USA). Depth was determined either from measured rope length (August 2017) or a pressure transducer (August 2018, May 2019). Approximately 30kg of metal weights (hammer heads) were attached below the sampler to ensure vertical position of the sampler relative to the boat. The samples were collected isokinetically, i.e. with the boat drifting with the flow. Once at the required depth, the sampler doors were pneumatically shut using a bicycle pump. Additional bedload samples were collected by dredging river bottom sediments using a weighted metal bucket.

Samples were collected into 10 L sterile polyethylene bags, ensuring complete transfer of all sediment particles. The bags were weighed and the samples filtered within 24h using 0.2 μm PES membrane. The sediments were immediately washed off the filter and into an opaque glass jar, using filtered river water collected at the same site. The samples were kept sealed in the dark during transport back to the lab (between 1 and 2 weeks). They were then allowed to settle and were decanted (except very clay-rich samples), followed by freeze-drying using a Thermo Scientific ModulyoD freeze dryer. Suspended sediment concentration was calculated by dividing the dried sample weight by the weight of the total water sample prior to filtration, ignoring the <1% error due to sediment mass (<10g / kg) in the original sample.

Particle size distributions of dried samples were measured using a Malvern Mastersizer 2000 laser diffractometer, at a 20-bin resolution ranging between 0.35-2000 μm . Each sample amount was adjusted to achieve 10-20% obscuration and ranged from 50 to 5000 mg, depending on the coarseness. Each sample was dispersed in tap water and sonicated for 2-5 min until grain size distribution appeared stable. Each measurement was repeated 3-5 times. Typical uncertainty was better than 10% for each grain size bin, with most of the uncertainty due to subsampling errors of the coarse particles.

To measure the organic carbon concentration (weight %), carbonate was removed from the samples by a liquid HCl phase, within capsules with no rinse step (Komada et al., 2008). In detail, crushed sediment powders were weighed (approx. 5-10 mg sample for suspended sediments and 20 mg for bedload, attempting a target mass of organic carbon of $\sim 100 \mu\text{g C}$) into 8×5 mm silver capsules that had previously been combusted

259 (450 °C for 4 hours, within 3 days of processing) and loaded open into a PTFE sample
 260 tray. Around 50 μL of 1N HCl was added to each capsule, with the liquid reactant evap-
 261 orated at 65 °C to dryness in an oven. Acid addition and drying was repeated three times
 262 in total. Capsules were folded close and analysed by EA-IRMS at Elementex with a range
 263 of international calibration standards and external standards (IAEA 600, IAEA CH3)
 264 and to check for full carbonate removal (NCS-DC73319). Measured %OC values were
 265 corrected for a full procedural blank (<5% of the sample carbon mass) and repeat mea-
 266 surements of samples and external standards had a precision of 0.05%.

267 **3 Revised hydrodynamic sediment transport model**

268 River sediment is transported in suspension when turbulent shear stress (which can
 269 be expressed as shear velocity) is sufficient to overcome the particle settling velocity (e.g.,
 270 Miller et al., 1977). Because turbulent shear stress affects all particles equally, whereas
 271 settling velocity depends on particle size, the ratio of these two parameters can theoret-
 272 ically predict how the concentration of particles of *a given size* would vary with depth
 273 (Rouse, 1950):

$$C_i(z_r) = C_0^i \cdot z_r^{R_i} \quad (1)$$

274 where

$$z_r = \frac{(H - z)/z}{(H - z_0)/z_0} \quad (2)$$

275 C_i is the sediment concentration in grain size class i and z_0 is a reference height,
 276 defined here as fixed fraction of total water depth $0.001 \cdot H$ (Lupker et al., 2011). The
 277 sediment concentration at this reference height is C_0^i . The "Rouse depth", z_r , is the sam-
 278 ple depth z , non-dimensionalized relative to the reference height z_0 and total water col-
 279 umn height H .

280 The power exponent in Eq. 1 is commonly referred to as the Rouse number:

$$R_i = \frac{w_i}{\beta \cdot \kappa \cdot u_*} \quad (3)$$

281 The value of R_i is dependent on particle settling velocity w_i of sediment grain size
 282 i , the ratio of sediment and water momentum diffusion coefficients, β , and shear veloc-
 283 ity u^* (see Supp. Text Eq. S2); $\kappa = 0.41$ is the von Karman constant. The higher R_i ,
 284 the stronger the increase in sediment concentration with depth.

285 Attempts to obtain R_i from fully theoretical considerations have so far been un-
 286 successful, due to a number of reasons. Firstly, it is difficult to accurately determine par-
 287 ticle settling velocity, especially for natural sediments composed of mixtures of mineral
 288 and organic matter of variable density and shapes (Dietrich, 1982), with potential par-
 289 ticle aggregation adding further complication (Bouchez, Métivier, et al., 2011). Secondly,
 290 while many simpler treatments take β to be equal to 1, experimental data have shown
 291 it to vary considerably with sediment concentration (Muste et al., 2005), likely the rea-
 292 son for the complex variations in β observed in real rivers (Lupker et al., 2011). For these
 293 reasons, previous workers were unable to apply Eq. 3 to large rivers, instead turning to
 294 empirical calibration of R_i using measured variations in sediment concentration with depth
 295 (Eq. 1) (Bouchez, Métivier, et al., 2011; Lupker et al., 2011).

296 In these previous applications of the Rouse model to large rivers, Eq. 1 was used
 297 to either obtain one average R_i across a river channel, effectively averaging laterally (Bouchez,
 298 Métivier, et al., 2011; Bouchez, Lupker, et al., 2011), or applied to depth profiles collected
 299 under varying hydrodynamic conditions and establishing an empirical fit between depth-
 300 averaged sediment flux and u^* (Lupker et al., 2011). In other words, Bouchez, Métivier,
 301 et al. (2011) and Bouchez, Lupker, et al. (2011) applied a single shear velocity value per
 302 cross-section, therefore only integrating the geometry of the channel to calculate the flux,
 303 without modeling the lateral variation in hydrodynamic conditions. This approach worked
 304 well for Bouchez et al. because they were modeling very deep (up to 60 m) river chan-
 305 nels in relatively straight sections of the Amazon River and its major tributaries, where
 306 the lateral variation in shear velocity was minimal. This, however, is not the case for many
 307 rivers with more complex channel cross-section morphologies, such as the lower Irrawaddy
 308 and Salween rivers studied here (Fig. 2).

309 In contrast, Lupker et al. (2011) collected eight sediment sample depth profiles (n
 310 $= 3-9$ per profile) at the same site on the Ganges River, but under strongly varying hy-
 311 drodynamic conditions over the course of several years. They then applied Eq. 1 indi-
 312 vidually to each depth profile, obtaining a vertically integrated sediment flux, relating

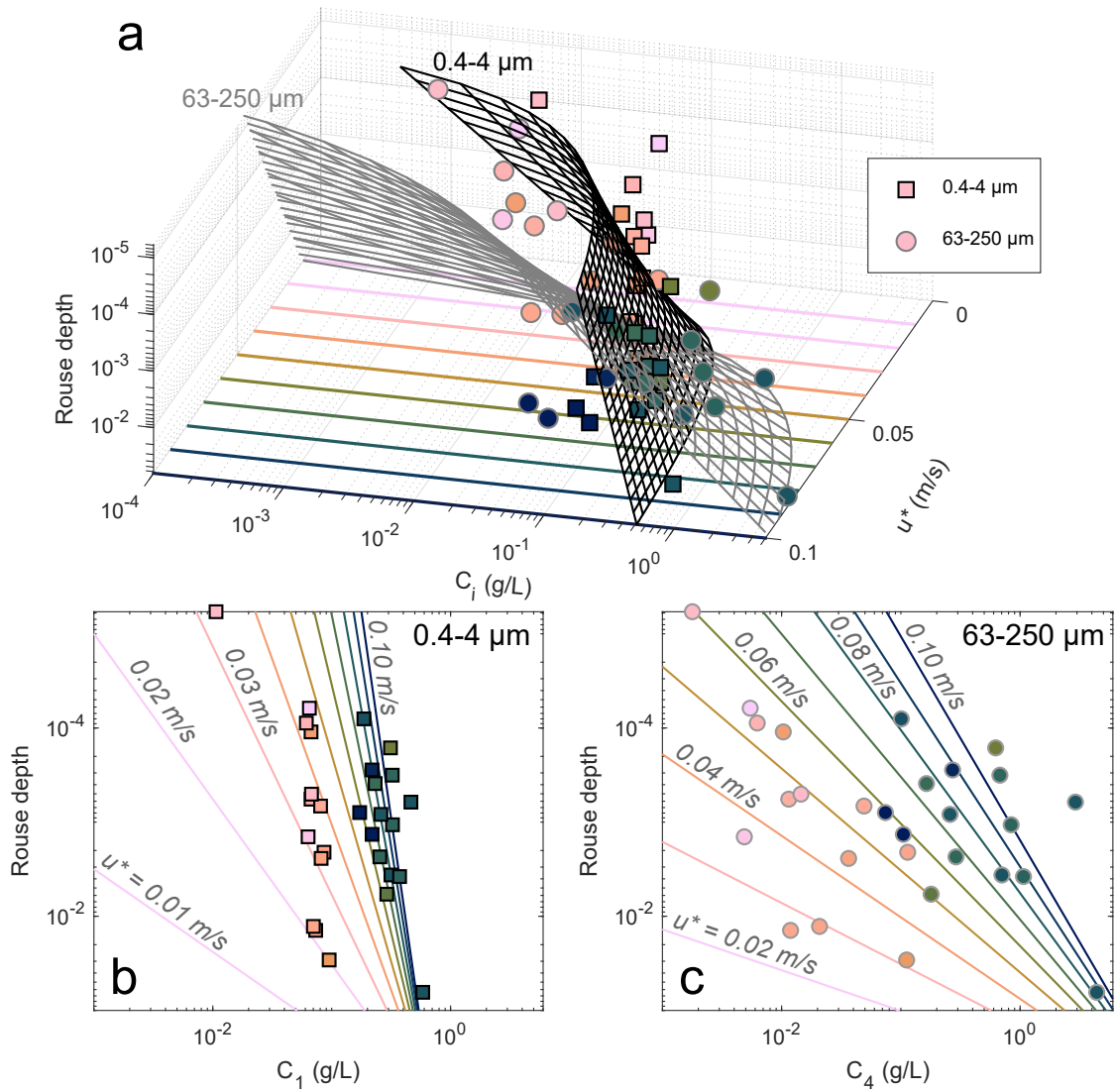


Figure 3. An example of three-dimensional fits to Eq. 4 (gridded curved surfaces in panel a) for two grain size fractions of measured Salween River suspended sediment concentrations (circles and squares). Rouse depth (z_r , as defined in Eq. 2) equals 1 at the river bed and 0 at the water surface. Panels b and c show the same fits and sample data in 2D representation separately for each grain size fraction. The colored lines in the bottom panels are projections (or "slices") of the three-dimensional gridded surfaces shown in (a) at selected u^* values, as indicated by the colored lines in (a). The sample symbols are also colored according to u^* associated with each sample (Supp. Table S1).

313 it to local u^* , and then using this relationship to laterally and temporally extrapolate
 314 the vertically-integrated sediment flux. While robust, this approach requires a large num-
 315 ber of suspended sediment samples and was enabled by a continuous field effort over the
 316 period of several years, and is therefore not ideal for the smaller sample set of our study.

317 Here, we employ a different approach from these previous studies to address the
 318 highly dynamic flow conditions of the rivers studied here, while using a smaller number
 319 of sediment depth samples. We do this by explicitly factoring u^* out of the fitted expo-
 320 nent in the Rouse equation:

$$C_i(z_r, u^*) = C_0^i \cdot z_r^{b_i/u^*} \quad (4)$$

321 where z_r is calculated from sample depth recorded during collection, u^* is calcu-
 322 lated from the depth-integrated flow velocity during sample collection (see Supp. Text
 323 S1 for details), and C_0^i and b_i are fitted parameters (obtained separately for each grain
 324 size bin i).

325 Because b_i is strongly dependent on sediment grain size, and grain size distribu-
 326 tion is known to vary widely with depth and hydrodynamic conditions in large rivers,
 327 measured sediment concentrations are divided into five grain size bins ($i = 0.2-4, 4-16,$
 328 $16-63, 63-250, 250-2000 \mu m$) and Eq. 4 is then fitted individually to each one (Fig. 3;
 329 see Supp. Text S1). The empirically calibrated C_0^i and b_i values can then be applied to
 330 ADCP-measured velocity data to calculate and map high-resolution variations in sed-
 331 iment concentration C_i with depth and across the river channel (Fig. 4). Combining the
 332 five C_i values also yields the variation in sediment grain size across the channel (Fig.4).
 333 The suspended sediment flux [$kg m^{-2} s^{-1}$] distribution across the channel is then cal-
 334 culated for each ADCP data bin as

$$q_s(z, x) = \sum_i C_i(z, x) \cdot u(z, x) \quad (5)$$

335 which can be summed up to obtain the total instantaneous suspended sediment flux
 336 [$kg s^{-1}$]:

$$Q_S = \sum_{z,x} q_s(z, x) \cdot A(z, x) \quad (6)$$

337 where z and x are the bin coordinates in vertical (depth) and horizontal (lateral
 338 distance across the channel) direction, respectively, u is flow velocity, and A is the cross-
 339 sectional area of a given ADCP bin (e.g., 0.25 m \times 0.5 m).

340 In summary, the method described here has certain advantages over previous ap-
 341 plications of the point sampling approach to integrate sediment variation with depth in
 342 large rivers:

- 343 1. Despite the additional degree of freedom (u^*) in the regression model (Eq. 4), it
 344 utilizes all sample data simultaneously ($n = 30-37$ in our case), rather than fit-
 345 ting sediment depth profiles one-by-one as done by Lupker et al. (2011) ($n = 3-$
 346 9), therefore improving the overall error minimization of the model fit to the data.
- 347 2. Because it relies on the Rouse equation, it does not require the explicit calibra-
 348 tion of the ADCP sonar equation (Kostaschuk et al., 2005; Darby et al., 2016; Szu-
 349 piany et al., 2019) and different ADCP instruments can be used to obtain flow ve-
 350 locity measurements during different field campaigns.
- 351 3. It enables a two-dimensional synoptic map of sediment concentration, flux, and
 352 grain size distribution across morphologically complex river channels, where depth
 353 and flow velocity often show significant lateral variations (Fig. 4) and where av-
 354 eraging across the channel (Bouchez, Lupker, et al., 2011; Morin et al., 2018; San-
 355 tini et al., 2019) would likely result in significant errors of the calculated sediment
 356 flux and mean composition.

357 The above model applies only to sediment transported in suspension, and does not
 358 include sediment carried as bedload below the reference height z_0 . To calculate the bed-
 359 load flux, we adopted the semi-empirical bedload transport equation of van Rijn et al.
 360 (2007), as previously employed by Lupker et al. (2011), described in detail in Supp Text
 361 S2. The total instantaneous and time-averaged sediment flux values reported below are
 362 given as the sum of the suspended and the bedload sediment fluxes.

363 The sediment modeling procedure described above was applied to the Irrawaddy
 364 and the Salween rivers separately, calculating the mean sediment concentration, grain
 365 size, and %OC distribution, as well as the total instantaneous sediment and POC flux
 366 for each of the four ADCP cross-sections measured at each site. The results are summa-

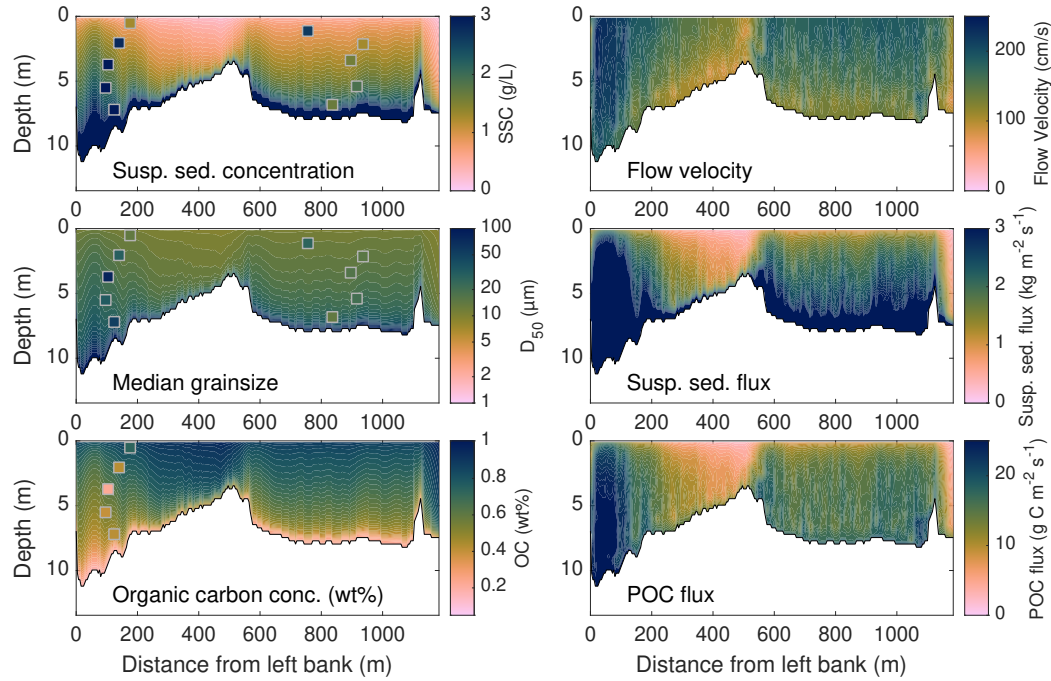


Figure 4. Results of the hydrodynamic sediment transport model for Salween at Hpa-An (2018 August 24), showing the depth and lateral variability in sediment composition and flux. The square colors reflect the measured sample compositions that were used to calibrate the model, demonstrating the model’s ability to recover the initial values. Results for the other cross-sections are given in the Supp. Material.

367 rized in Table 1 and the figures equivalent to Fig. 4 for the other seven cross-sections
 368 are given in the Supplementary Material.

369 **4 Results**

370 The measured water discharge of the Irrawaddy and the Salween at each of the four
 371 sampling dates are given in Table 1. Measurements were performed at the peak of the
 372 monsoon season, as well as in mid- and late dry season, and therefore span about an or-
 373 der of magnitude range in discharge ($3000\text{--}42100\text{ m}^3/\text{s}$ for the Irrawaddy and $1800\text{--}14300$
 374 m^3/s for the Salween). Importantly, these values bracket almost the full range of monthly
 375 mean discharge for both rivers (Supp. Table S4), allowing us to interpolate the results
 376 of this study for each month, yielding long-term average sediment composition and an-
 377 nual flux (see discussion below and Supp. Text S3).

Table 1. Measured instantaneous discharge and modeled sediment flux and composition of the Irrawaddy and Salween rivers.

River (site)	Date	Discharge (m ³ /s) *	Sed. samples	Hydrodynamic model results						
				Sed. flux (kg/s)	Sed. flux (Mt/d)	Mean SSC (mg/L)	Mean D ₅₀ (μ m)	Mean D ₈₄ (μ m)	Mean OC (wt%)	POC flux (10 ⁹ g C/d)
Irrawaddy (Pyay)	2017-08-23	42100	n = 10	56300 \pm 5600	4.9 \pm 0.5	1340 \pm 130	41 \pm 6	219 \pm 22	0.23 \pm 0.13	11.0 \pm 1.1
	2018-02-03	3000	n = 1	720 \pm 140	0.063 \pm 0.013	240 \pm 50	10 \pm 1	71 \pm 19	0.58 \pm 0.15	0.36 \pm 0.07
	2018-08-22	32100	n = 11	45500 \pm 4430	3.9 \pm 0.4	1360 \pm 130	43 \pm 6	228 \pm 35	0.22 \pm 0.13	8.7 \pm 0.8
	2019-05-21	5300	n = 15	1490 \pm 280	0.13 \pm 0.02	280 \pm 50	11 \pm 1	93 \pm 15	0.55 \pm 0.14	0.70 \pm 0.13
Salween (Hpa-An)	2017-08-21	11900	n = 7	25200 \pm 2980	2.2 \pm 0.3	2120 \pm 250	32 \pm 3	165 \pm 7	0.46 \pm 0.25	10.0 \pm 1.2
	2018-02-01	1800	n = 1	400 \pm 110	0.035 \pm 0.009	230 \pm 60	11 \pm 1	37 \pm 2	0.90 \pm 0.30	0.31 \pm 0.08
	2018-08-24	14300	n = 10	25200 \pm 3060	2.2 \pm 0.3	1760 \pm 210	25 \pm 2	136 \pm 8	0.53 \pm 0.26	12.0 \pm 1.4
	2019-05-19	2700	n = 12	1230 \pm 250	0.11 \pm 0.02	460 \pm 90	12 \pm 1	41 \pm 2	0.85 \pm 0.29	0.9 \pm 0.18

*Based on repeat transects, uncertainty better than 6% and in most cases better than 2%.

378 The measured suspended sediment concentrations (SSC) ranged from 55 to 5500
379 mg/L in the Irrawaddy and 47 to 10200 mg/L in the Salween (all individual sample de-
380 tails and measured values are given in the Supp. Table S1). The median grain size (D_{50})
381 ranged from 5 to 150 μ m in the Irrawaddy and 8 to 130 μ m in the Salween. The most
382 concentrated (and coarsest) samples were collected during the monsoon and typically
383 closer to the channel bottom, indicating the influence of hydrodynamic sorting. How-
384 ever, a significant number of coarse, high-concentration samples in both rivers were col-
385 lected at mid-depth (Fig. 5). Because our depth sampler collects instantaneous samples
386 without time-averaging, the variable vertical dispersion of sand in our samples reflects
387 the complexity of hydrodynamics in these rivers (e.g., non-steady state turbulent sed-
388 iment suspension events, secondary flow, bedform effects, etc.). As discussed above, this
389 complexity prevents simple spatial averaging with depth or across the river channel to
390 calculate the total sediment flux and requires a fully spatially-resolved sediment trans-
391 port model (Section 3).

392 To estimate the flux of particulate organic carbon (POC) by these rivers, we anal-
393 ysed the organic carbon concentration in a subset of the suspended sediment samples.
394 As in many other rivers, in the Irrawaddy and Salween most organic carbon is associ-
395 ated with finer particles, and sediment OC (wt%) is closely correlated with median sed-
396 iment grain size (Fig. 6). This relationship can be used to convert the spatial D_{50} di-
397 stribution into %OC and subsequently, the POC flux (Fig. 4) can be calculated using equa-
398 tions equivalent to Eqs. 5 and 6.

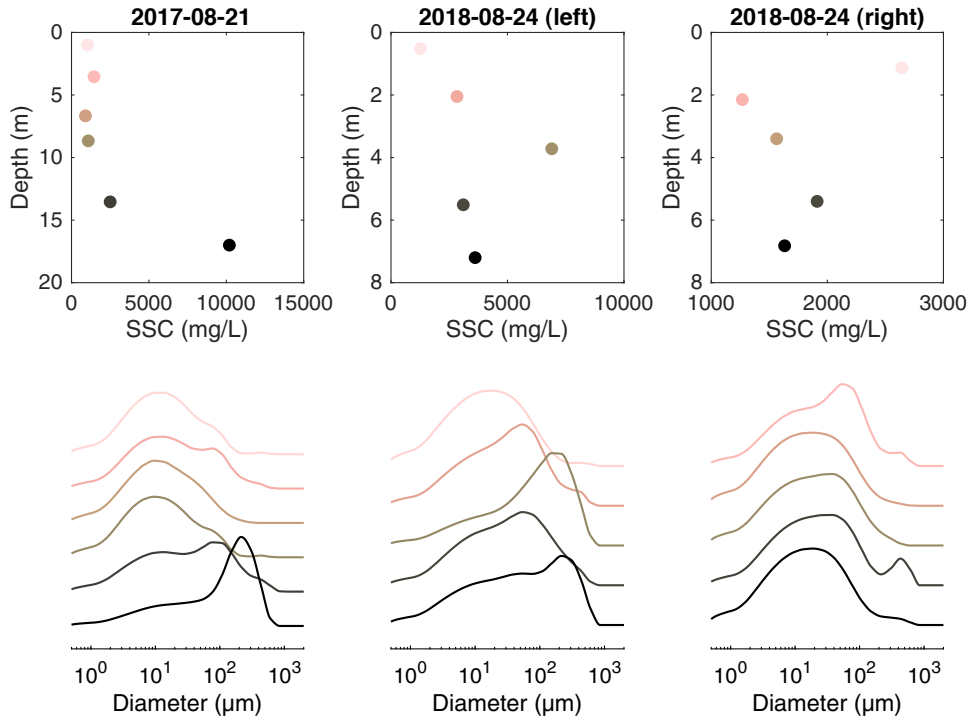


Figure 5. An example of measured variations in SSC (upper panels) and grain size distributions (lower panels, shown as relative probability density functions) with depth (darker colors reflecting deeper samples) at three locations across the Salween river channel during high discharge stage. The two profiles on 2018-08-24 correspond to the samples collected on the left and the right side of the channel, respectively, as shown in upper left panel of Fig. 2.

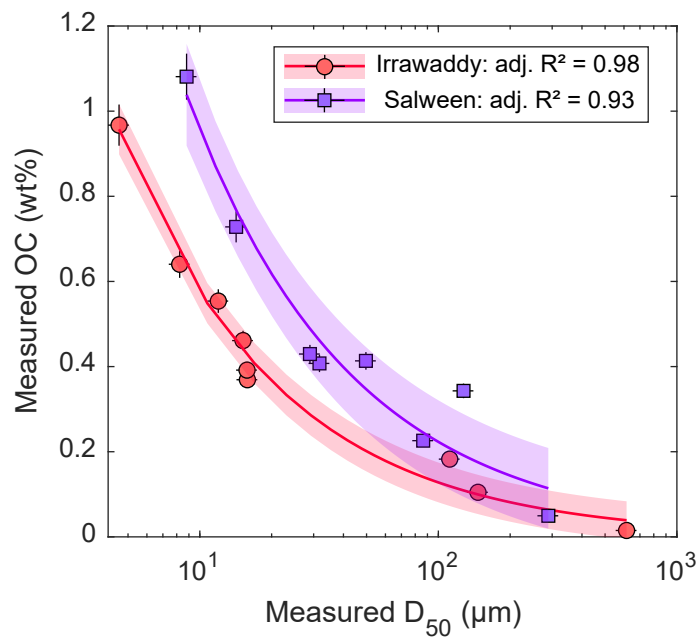


Figure 6. Relationship between measured sediment median grain size (D_{50}) and organic carbon content in each river, using samples collected across all seasons (incl. bedload). The dashed lines show power-law fits: $\%OC = (2.59 \pm 0.28)D_{50}^{(-0.65 \pm 0.05)}$ for Irrawaddy and $\%OC = (4.11 \pm 0.97)D_{50}^{(-0.63 \pm 0.08)}$ for Salween, with parameter uncertainties given as 68% confidence intervals.

5 Discussion

5.1 Instantaneous sediment flux and composition

The calculated total instantaneous sediment flux ranged from 700 to 56,000 kg/s and from 400 to 25,000 kg/s for the Irrawaddy and the Salween, respectively (Table 1). The grain size distribution was generally coarser and more variable in the Irrawaddy (D_{50} range 10-43 μm) relative to the Salween (D_{50} range 11-32 μm). Although the Irrawaddy discharge and sediment flux is about 50% higher than the Salween, due to the higher %OC of Salween sediments, the POC fluxes were similar in both rivers, ranging from 0.3 to $12 \cdot 10^9$ g C / day. The calculated bedload sediment flux ranged from 11 to 1500 kg/s in the Irrawaddy and 6 to 740 kg/s in the Salween, representing only 1-3% of the total sediment flux in each case, regardless of the hydrodynamic conditions. These results agree well with the similarly small portion ($\sim 1.5\%$) of total sediment flux carried in the bedload in the Ganges River (Lupker et al., 2011), as well as the Mekong River (Hackney et al., 2020), both similar in size to the Irrawaddy in their lower reaches. The total instantaneous (Table 1), monthly (Fig. 7; Supp. Table S4), and annual (Table 2) sediment flux values are all given as the sum of the suspended and the bedload sediment fluxes. The bedload POC flux is ignored, given that coarse sand contains low %OC (Fig. 6) and that the majority of sediment is carried as suspended load, this approximation should result in a negligible underestimation of the total POC flux.

5.1.1 The performance of the hydrodynamic sediment transport model

To assess the performance of the model, the measured sample compositions can be compared to values calculated using the model at the equivalent locations (depth and lateral) in each channel cross-section. An example of a visual comparison between the measured and calculated parameters for the Salween in August 2018 is given in Fig. 4, with other cross-sections shown in Supp. Material. A more detailed comparison is shown for all sediment samples at both sites in Fig. 8. The degree of misfit between measured and modeled values (represented as a mean relative standard error) was less than 5% for SSC and D_{50} in both rivers, while the %OC relative standard error was -35% for the Irrawaddy and +30% for the Salween. The higher and more systematic misfit of %OC is likely due to the considerably smaller number of data available to calibrate the model (Figs. 6, 8c) compared to SSC and D_{50} and should be improved with additional anal-

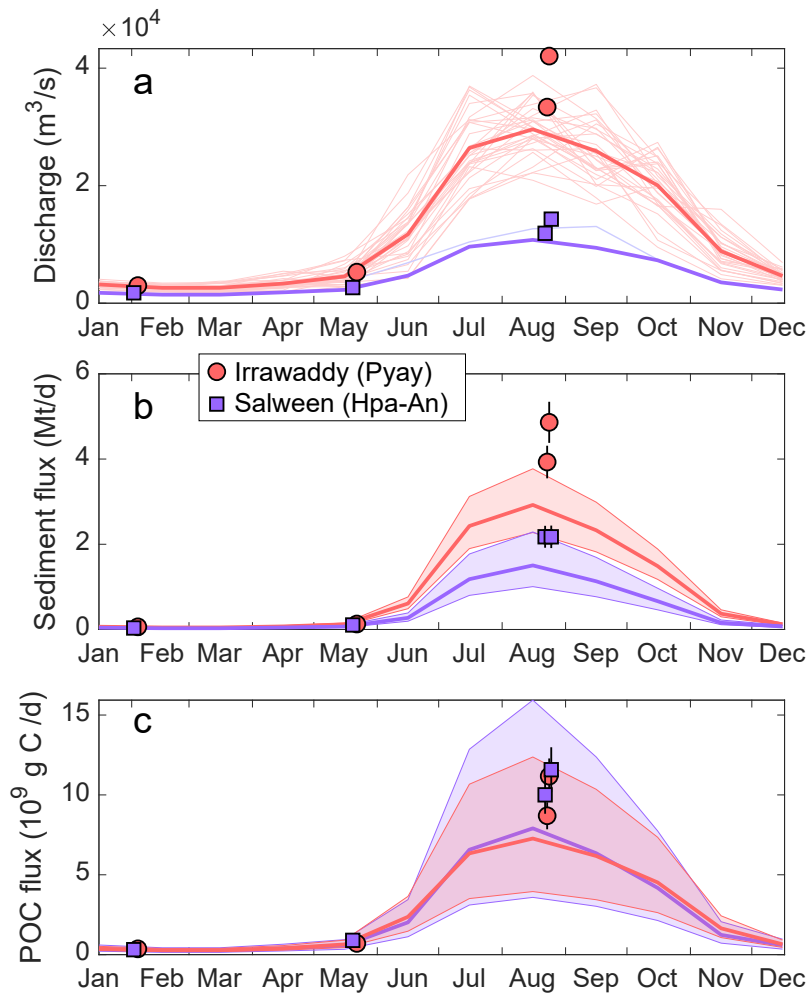


Figure 7. Average monthly discharge (a), sediment (b), and particulate organic carbon (c) fluxes in the Irrawaddy and Salween rivers. Our ADCP-measured discharge and Rouse-calculated flux values are shown as circles and squares for the Irrawaddy and Salween, respectively (see Section 5.1.1). Thin lines in (a) show discharge data reported by the Department of Hydrology and Meteorology in Myanmar (1966-1996 for the Irrawaddy; May-Oct 2004 for the Salween, previously published by Furuichi et al. (2009) and Chapman et al. (2015), respectively). For discharge, the thick line represents the 31-year monthly averages for the Irrawaddy, whereas the Salween monthly discharge was calculated using the Irrawaddy/Salween discharge ratio determined in the wet and dry seasons in this study (see Supp. Text S3 for details). In (b) and (c), the thick line shows the best estimate with shaded area as the 68% confidence interval propagated through all calculations (see Supp. Text S3).

430 yses. We also note that this is not a strict test of the model, as it uses the training dataset
 431 to assess the performance. A more rigorous assessment can be performed in the future
 432 against similar additional datasets (i.e., sediment samples coupled to ADCP flow veloc-
 433 ity measurements) at these sites.

434 We propose that there are three main reasons for the misfit between the modeled
 435 and the measured values:

- 436 1. In some cases, large deviations from expected sediment sorting were observed, with
 437 several coarse, high-SSC samples collected at mid-depth (Fig. 5), likely due to non-
 438 steady state suspension events during sampling as discussed above.
- 439 2. There is some degree of mismatch between the ADCP velocity measurements (which
 440 integrate over a increasingly larger horizontal area with increasing depth) and the
 441 exact location of the collected sediment samples.
- 442 3. The location and the shape of the channel cross-section varied slightly from year
 443 to year at both sites (Fig. 1b,c; Supp. Figures).

444 These factors inject substantial noise into our sample set, resulting in an offset be-
 445 tween the sampled sediments and the local hydrodynamic conditions (represented by shear
 446 velocity) assigned to each sample (see Supp. Text S1). Finally, an additional source of
 447 uncertainty is the possible change in sediment supply to each river (e.g., seasonal hys-
 448 teresis, or inter-annual variations caused by landsliding or land-use changes upstream)
 449 during the time-span over which samples were collected for this study. However, such
 450 effects are typically local and we expect them to be minor compared to the immediate
 451 turbulence-induced noise (point no. 1 above), and to be mostly averaged out on the large
 452 basin-scale considered here. Ultimately, the spatial distribution of sampled sediment com-
 453 position cannot be fully reconciled using a model that implicitly assumes constant sed-
 454 iment supply, constant channel structure, and equilibrium hydrodynamic conditions. De-
 455 spite these complications, the sediment transport model presented here recovers the ini-
 456 tial sample sediment composition for both the Irrawaddy and the Salween, without any
 457 large systematic errors (Fig. 8). The relative standard error (i.e., the mean residual of
 458 measured vs. modeled values) was better than $\pm 5\%$ for both SSC and D_{50} (Fig. 8a-b)
 459 and was -35% for %OC in the Irrawaddy and $+30\%$ in the Salween (Fig. 8c), likely due
 460 the smaller number of available data and error propagation in the D_{50} -%OC calibra-
 461 tion (Fig. 6). The utility and need for such a model is further evaluated below, by com-

462 paring the flux and mean sediment composition values calculated here with estimates
 463 derived using simpler approaches.

Table 2. Properties of the river basins and the mean annual sediment composition and fluxes calculated in this study (see text). Except for elevation, the calculated values in parentheses represent a 68% confidence interval. The elevation and median slope were determined using the hydrologically conditioned MERIT HYDRO digital elevation model (Yamazaki et al., 2019).

	Irrawaddy	Salween	
<u>Basin properties</u>			<i>units</i>
Planimetric area	422,400	266,500	km^2
DEM surface area ^a	436,500	282,300	km^2
Mean elevation (range)	862 (0-5790)	3515 (0-6860)	<i>m</i>
Median slope	7.1	16.4	<i>degrees</i>
Geology	Marine silic. sedim., some metamorphic and igneous rocks; large central alluvial valley	Mixed limestones, granitoids, and metamorphic rocks	
<u>Results^b</u>			
ADCP discharge measurements	n = 4	n = 4	
Susp. sed. samples	n = 37	n = 30	
Water discharge ^c	379 ± 9	149	$km^3 yr^{-1}$
Runoff ^d	900 ± 20	560	$mm yr^{-1}$
Sed. flux	326 (256-417)	159 (109-237)	$Mt yr^{-1}$
POC flux	0.95 (0.55-1.55)	0.94 (0.46-1.79)	$Mt C yr^{-1}$
Erosion rate ^e	0.28 (0.22-0.35)	0.21 (0.14-0.31)	$mm yr^{-1}$
Sed. yield ^e	750 (590-960)	560 (390-840)	$t km^{-2} yr^{-1}$
POC yield ^e	2.2 ± 1.2	3.3 (1.6-6.3)	$t C km^{-2} yr^{-1}$
Mean SSC	0.9 (0.7-1.1)	1.1 (0.7-1.6)	$g L^{-1}$
Mean D ₅₀	28 (23-34)	21 (17-26)	μm
Mean D ₈₄	183 ± 13	112 ± 27	μm
Mean OC	0.29 ± 0.08	0.59 ± 0.16	<i>wt%</i>

^a Based on MERIT HYDRO DEM (Yamazaki et al., 2019), down-sampled to 90m resolution.

^b See Supp. Text for details of calculations.

^c Using previously published data from the Department of Meteorology and Hydrology in Myanmar (see Supp. Text).

^d Calculated using planimetric area.

^e Calculated using DEM surface area.

464 5.1.2 The need for a hydrodynamic sediment transport model

465 Our results indicate that, at least in the case of the Irrawaddy and the Salween,
 466 the sampled sediments frequently deviate from the expect Rousean behaviour, that is,
 467 sampled sand concentration does not always increase with depth (Fig. 5). It is there-
 468 fore reasonable to ask whether a Rouse-based hydrodynamic sediment transport model

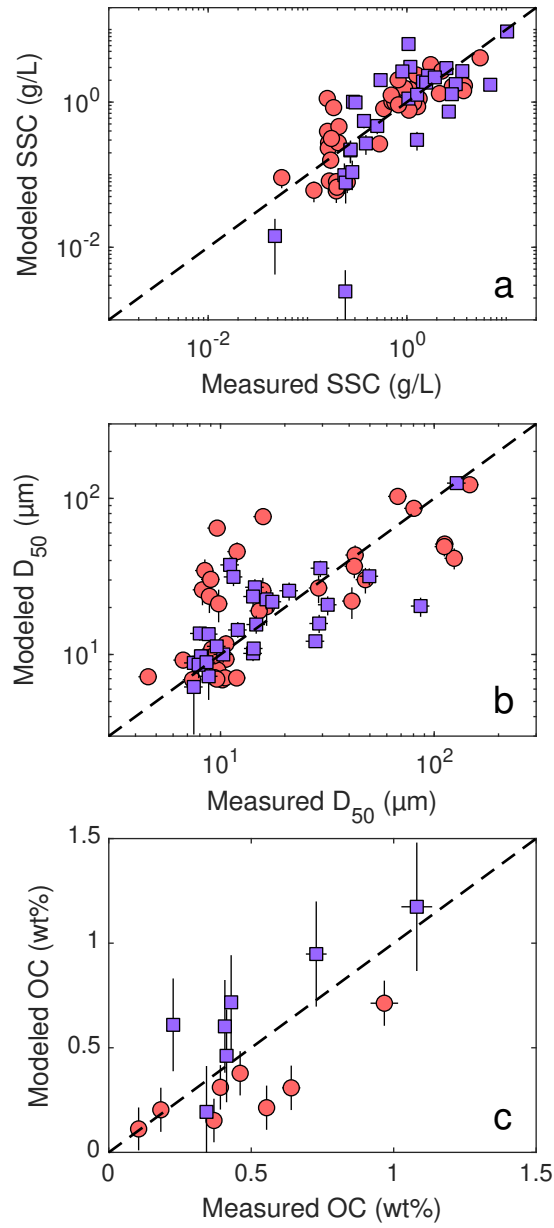


Figure 8. Comparison of measured sediment composition with values re-calculated using the sediment transport model described in Section 3 for all Irrawaddy (red circles) and Salween (purple squares) River samples. Dashed lines show 1:1 relationship. The horizontal error bars represent analytical uncertainty, while the vertical error bars were calculated using a 68% confidence interval of the Rouse model fit (Eq. 4; Fig. 3). Measured and recalculated values for all samples are given in the Supp. Table S1.

469 is required, and whether a simple averaging of all sediment samples, such as employed
470 previously by Robinson et al. (2007) for the Irrawaddy, would yield flux and mean sed-
471 iment composition estimates that are indistinguishable from the more complex hydro-
472 dynamic modeling approach employed in this study. A comparison of the instantaneous
473 sediment and POC fluxes, as well as mean grain size parameters calculated using the dif-
474 ferent approaches (including previously published rating curves and %OC values) is shown
475 in Table 3. Given that we collected sediment samples at roughly consistent depth per-
476 centiles (typically 5-25-50-75-95% or 5-50-95% of total depth), as well as at several dif-
477 ferent lateral locations across the channel, we consider our sample set to be reasonably
478 uniform in both dimensions of the channel cross-section. Taking a simple average of the
479 sampled SSC values and multiplying by the total ADCP-measured discharge has yielded
480 sediment flux estimates that ranged from ~40% lower during the dry season to ~50%
481 higher during the wet season, compared to Rouse model results for both rivers. Simi-
482 larly, the mean grain size parameters (D_{50} and D_{84}) were frequently over- or under-estimated,
483 depending on the particular cross-section, reflecting the fact that simple-mean estimates
484 fail to accurately account for sand transport in the near-bed region. Finally, using sim-
485 ple means of measured values significantly overestimated the POC flux by anywhere be-
486 tween 40 and 95% during the wet season for both rivers. Given the large size and dis-
487 charge of the two rivers, this would result in a non-negligible error of riverine carbon ex-
488 port on a globally relevant scale. This comparison shows how crucial it is to accurately
489 account for hydrodynamic sorting of sediments in large and morphologically and hydro-
490 dynamically complex rivers.

491 Although the chemical composition of the transported sediments is outside of the
492 scope of this study, similar averaging errors can significantly affect the calculated fluxes
493 of chemical elements which are highly sensitive to particle grain size, such as silicon (mostly
494 contained in coarser quartz sand grains) and aluminum and iron (mostly contained in
495 clay particles). These sorting bias effects were well exemplified and quantified on an element-
496 by-element basis by Bouchez, Gaillardet, et al. (2011) and Lupker et al. (2011) for the
497 Amazon and the Ganges rivers, respectively. Given the importance of hydrodynamic sort-
498 ing for the SSC and POC values in the Irrawaddy and Salween, we therefore expect sim-
499 ilarly significant bias in elemental (and isotopic) fluxes, to be explored in follow up stud-
500 ies.

Table 3. Comparison of hydrodynamic Rouse-based model results with simple mean-derived estimates using the sample set presented here, as well as previously published fluxes (Robinson et al., 2007; Bird et al., 2008).

Date	Parameter	Previous estimate ^a	Simple mean ^b	Rouse model ^c	Error ^d
<i>Irrawaddy (Pyay)</i>					
2017-08-23		3.5	7.4	4.9	52%
2018-02-03	Total sed.	0.06	0.04	0.06	-31%
2018-08-22	flux (Mt/d)	2.3	3.4	3.9	-13%
2019-05-21		0.14	0.08	0.13	-36%
2017-08-23		470	218	129	69%
2018-02-03	POC flux	11	--	4	--
2018-08-22	(kg/s)	308	157	97	62%
2019-05-21		26	--	8	--
2017-08-23		--	65	41	60%
2018-02-03	D ₅₀ (μm)	--	--	10	--
2018-08-22		--	23	43	-46%
2019-05-21		--	10	11	-11%
2017-08-23		--	216	219	-1%
2018-02-03	D ₈₄ (μm)	--	--	71	--
2018-08-22		--	134	228	-42%
2019-05-21		--	27	93	-71%
<i>Salween (Hpa-An)</i>					
2017-08-21		--	2.1	2.2	-2%
2018-02-01	Total sed.	--	0.02	0.03	-38%
2018-08-24	flux (Mt/d)	--	3.3	2.2	52%
2019-05-19		--	0.08	0.11	-29%
2017-08-21		227	226	116	95%
2018-02-01	POC flux	26	--	4	--
2018-08-24	(kg/s)	227	185	134	38%
2019-05-19		26	--	11	--
2017-08-21		--	35	32	9%
2018-02-01	D ₅₀ (μm)	--	--	11	--
2018-08-24		--	31	25	21%
2019-05-19		--	9	12	-23%
2017-08-21		--	105	165	-37%
2018-02-01	D ₈₄ (μm)	--	--	37	--
2018-08-24		--	114	136	-17%
2019-05-19		--	43	41	5%

^a Sediment and POC fluxes recalculated for instantaneous discharges measured in this study (Table 1), using the SSC rating curve determined by Robinson et al. (2007) and the season-average wt% OC determined by Bird et al. (2008)

^b Calculated as product of discharge and a simple mean of SSC and POC for all samples collected and analyzed on a given date, where $n > 1$ (Table S1).

^c Calculated using the Rouse modelling approach described in Section 3.

^d Calculated as the relative difference between the simple mean-calculated value and the Rouse model-calculated value.

5.2 Temporal integration of sediment flux and composition

The mean SSC and POC values calculated at the four different sampling dates and discharge (Q_w) conditions for each river allowed SSC- Q_w rating curves to be constructed (Fig. 9). Using previously published monthly Irrawaddy discharge data over a 31-year period (1966-1996) (Furuichi et al., 2009), we can calculate the monthly sediment and POC fluxes (Fig. 7) and mean sediment concentration, grain size, and organic carbon content (Fig. 10), which can then be summed to obtain long-term average annual values, summarized in Table 2. Unfortunately, other than our measurements presented here, the only Salween discharge data available cover a period between May-Oct in 2004, previously published by Chapman et al. (2015). The only annual discharge value available for the Salween is $210 \text{ km}^3/\text{y}$ given by Meybeck and Ragu (1997), which has since been used in a number of publications on rivers in Myanmar, as well as global compilations of water, sediment, and chemical fluxes (e.g., Gaillardet et al., 1999; Robinson et al., 2007; Chapman et al., 2015). For this reason, we used our ADCP-measured discharge values, along with the average monthly Irrawaddy discharge, to re-estimate the monthly discharge of the Salween in proportion to Irrawaddy discharge, yielding a revised annual Salween discharge of $149 \text{ km}^3/\text{y}$ (see Supp. Text S3 for details).

Applying the rating curves shown in Fig. 9 to the monthly discharge timeseries, we are able to calculate the monthly suspended sediment and particulate organic carbon concentrations, median grain size (Fig. 10) and the sediment and POC fluxes (Fig. 7; all values given in Supp. Table S4). As expected, the sediment composition and flux varies by more than an order of magnitude in both rivers, with the coarsening of the transported sediment and the highest fluxes during the monsoon: monthly mean SSC ranged from 0.20 to 1.1 g/L in the Irrawaddy and from 0.22 to 1.6 g/L in the Salween, with annual flux-weighted means of 0.9 ± 0.2 and $1.1_{-0.4}^{+0.5}$ g/L, respectively (1σ uncertainty; Table 2). Overall, the Salween sediments are finer (D_{50} from 11 to 25 μm , compared to the Irrawaddy's 10 to 42 μm , with flux-weighted annual means of 21_{-4}^{+5} and 28_{-5}^{+6} μm , respectively).

Due to its lower discharge, the Salween sediment flux of 159_{-51}^{+78} Mt/y is about half of the Irrawaddy's 326_{-70}^{+91} Mt/y, with bedload comprising $\sim 2\%$ of each. However, because organic carbon concentration in the Salween is about twice that of the Irrawaddy

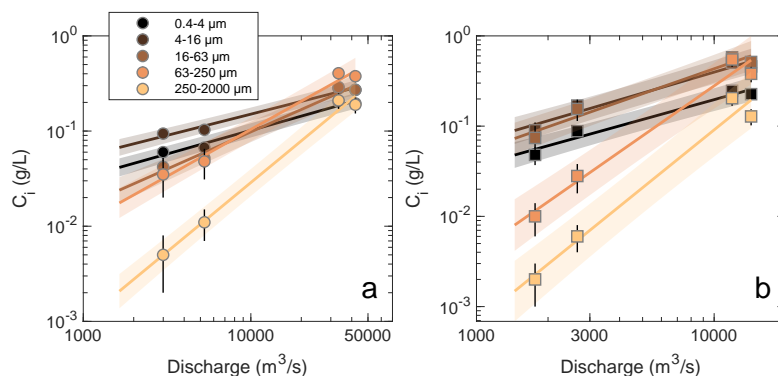


Figure 9. Rating curves used to calculate monthly and annual sediment average composition and flux for the Irrawaddy River at Pyay (a) and the Salween River at Hpa-An (b). The symbols show the mean suspended sediment concentrations calculated using the hydrodynamic sediment transport model, for five different grain size fractions (Section 3, Table 1). The lines and envelopes show best fit and 68% confidence interval of the fit. The fitted rating curves and the goodness-of-fit statistics are given in Supp. Materials.

532 (0.59±0.13 vs. 0.29±0.08 %), both rivers deliver a similar POC flux of ~1 Mt C/yr to
 533 the ocean.

534 5.3 Comparison to previously published annual flux estimates

535 Compared to other major global rivers, prior to this study there existed very lit-
 536 tle modern data on the water and sediment discharge in the Irrawaddy and the Salween.
 537 The most significant dataset was published in the 19th century by Gordon (1880), pre-
 538 senting 10 years of discharge and suspended sediment measurements on the Irrawaddy
 539 at a location close to our sampling site at Pyay. More recently, Robinson et al. (2007)
 540 collected additional sediment depth samples and re-evaluated the original Gordon dataset,
 541 determining annual estimates of water discharge of $422\pm 41 \text{ km}^3/\text{y}$ and sediment flux of
 542 $364\pm 64 \text{ Mt}/\text{y}$. Subsequently, Furuichi et al. (2009) used 31 years of discharge data pub-
 543 lished by the Department of Hydrology and Meteorology (DHM) in Myanmar (the same
 544 dataset was used in this study) to calculate annual discharge of $379\pm 47 \text{ km}^3/\text{y}$, where
 545 the uncertainty was given as 1 standard deviation of inter-annual variability and is there-
 546 fore an overestimate of actual uncertainty on the long-term average, which we recalcu-
 547 late here as 1 standard error of the mean, equal to $9 \text{ km}^3/\text{y}$ (Table 2) for the same 31

548 year period. Furuichi et al. (2009) further used a sediment rating curve for the Irrawaddy
549 developed by DHM to estimate an annual sediment flux of 325 ± 57 Mt/y, in good agree-
550 ment with our results. However, it must be noted that neither the sampling protocol nor
551 the data used to establish the rating curve given in Furuichi et al. (2009) are publicly
552 available.

553 Similarly, we revised the Salween sediment flux from 180 Mt/y previously estimated
554 by Robinson et al. (2007) using the Irrawaddy sediment rating curve, down to 159^{+78}_{-51}
555 Mt/y, using the first rating curve for the Salween, presented here. We note that discharge
556 monitoring of the Salween is necessary to further improve this estimate.

557 Finally, our determined annual POC fluxes are significantly lower than the values
558 previously presented in Bird et al. (2008): 0.55-1.55 vs. 2.2-4.3 Mt C/y for the Irrawaddy
559 and 0.46-1.79 vs. 2.4-3.4 Mt C/y for the Salween, a two-to-five-fold reduction in each
560 case. It is partly explained by the reduction in water discharge estimates but the main
561 reason appears to be significantly lower %OC measured in this study (Table 2, also see
562 Supp. Material for individual sample values), compared to the values determined by Bird
563 et al. (2008). One possibility is that this difference represents an actual decrease in %OC
564 over the past decade. However, a change of this magnitude is difficult to defend, con-
565 sidering the large area of both river basins, and the fact that the difference is of simi-
566 lar order for both rivers. We suggest that this discrepancy is likely the result of sampling
567 methodology differences between Bird et al. (2008) and the present study. Bird et al. (2008)
568 used a 2L horizontal Van Dorn sampler, collecting sediment samples at 1 m depth from
569 the surface, mid-depth, and 1 m depth from the bottom, measuring OC of 1.1-1.6 wt%
570 during high-discharge monsoon conditions, with similar values in both Irrawaddy (at Pyay)
571 and Salween (at Hpa-An) and almost constant throughout the water column, suggest-
572 ing negligible hydrodynamic sorting. This observation is in stark disagreement with both
573 the results presented in this study, as well as the similar increase in SSC with depth ob-
574 served by Gordon (1880). Although it is difficult to determine the exact reason for this
575 discrepancy, we speculate that sand may not have been adequately sampled by the smaller
576 2L volume sampler used by Bird et al. (2008) (vs. our 8.5L sampler, where we took ex-
577 treme care to rinse out and collect all sand particles during sample transfer). This re-
578 inforces why thorough depth sampling and sediment flux modeling that accounts for hy-
579 drodynamic sorting is crucial for accurate flux estimates in large rivers, especially for el-

580 elements such as carbon, whose concentrations are strongly coupled to sediment grain size
 581 (Fig. 6).

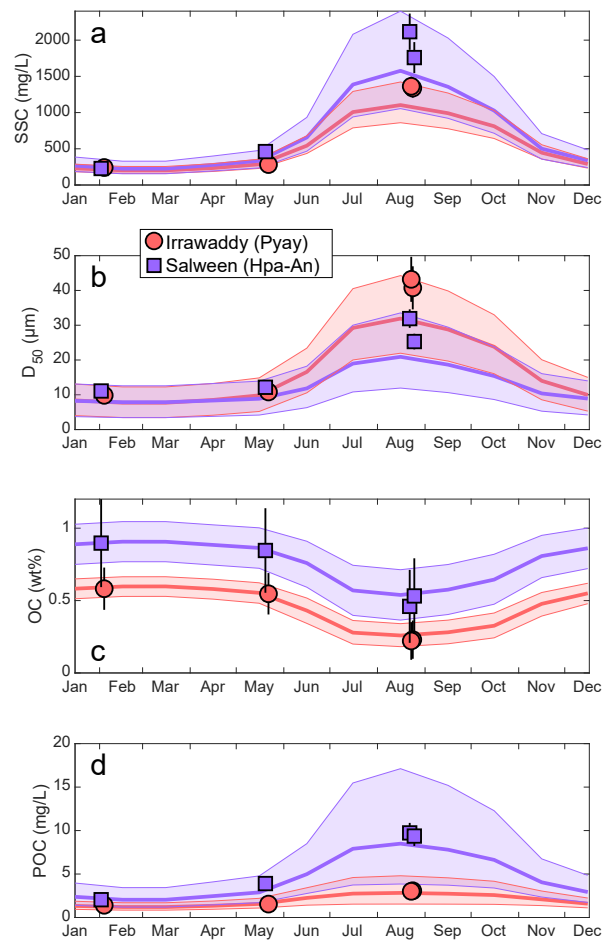


Figure 10. Average monthly SSC (a), median grain size D_{50} (b), organic carbon wt% (c), and POC concentration (d) in the Irrawaddy and Salween rivers. Our model-calculated flux values that were used to construct rating curves are shown as circles and squares for the Irrawaddy and Salween, respectively (see Section 5.1.1, Table 1). The thick line shows the best estimate with a 1σ uncertainty indicated by the envelope. Details of calculations are given in Section 5.2 and Supp. Text S3 and the calculated monthly values are given in Supplementary Material.

582 **5.4 Global significance of the Irrawaddy-Salween system**

583 Globally, using the values presented in this study, the Irrawaddy and the Salween
 584 exhibit some of the highest sediment fluxes (fifth and seventh worldwide, respectively;

585 Fig 11) and area-normalized sediment yields (third and fourth, respectively, among world's
586 30 major global rivers with annual discharge $> 100 \text{ km}^3 \text{ y}^{-1}$ as compiled by Milliman
587 and Farnsworth (2011), and lower only than the Fly and Brahmaputra rivers). Compared
588 to the nearby Ganges-Brahmaputra system, which is the main conveyor of Himalayan
589 erosion products to the ocean, the Irrawaddy-Salween system sediment yield is very sim-
590 ilar and sediment flux is about 46% that of Ganges-Brahmaputra. In comparison, the
591 Mekong River, also originating in the eastern Himalayan Syntaxis, used to deliver ~ 150
592 Mt y^{-1} (Milliman & Farnsworth, 2011), which has decreased to $87 \pm 28 \text{ Mt y}^{-1}$ (~ 2
593 and ~ 4 lower than the current fluxes of the Salween and the Irrawaddy, respectively) over
594 the past several decades due to damming and changes in precipitation across the basin
595 (Darby et al., 2016).

596 Although it is difficult to assess the global significance of the Irrawaddy-Salween
597 system due to uncertainty of the global sediment flux, comparing to the estimate of Milliman
598 and Farnsworth (2011), the two rivers are an important source of sediment to the ocean,
599 delivering 2-3% of the 19,000 Mt y^{-1} total sediment and 0.8-1.2% of the 200 Mt C y^{-1}
600 total (biospheric and petrogenic) POC (Galy et al., 2015) export to the ocean. It must
601 be noted, however, that current sediment flux estimates may be inaccurate for a num-
602 ber of large global rivers, where values are derived from sparse sample sets, often of sur-
603 face sediments only, lacking the depth sampling and hydrodynamic data required to ob-
604 tain robust values. The significance of our results is further underlined by the fact that
605 the Irrawaddy and the Salween are some of the last large rivers basins still relatively un-
606 affected by damming. Only a few small dams have been built on some minor tributaries
607 of both rivers, with their mainstems flowing freely from source to outlet (worldwide, the
608 only other megarivers with free-flowing mainstems are the Amazon and the Congo; Grill
609 et al. (2019)). Currently, the main anthropogenic pressures on these river basins, such
610 as deforestation, agriculture, and sand mining, are likely to be net erosive, enhancing the
611 sediment flux (Syvitski et al., 2005). However, large dams are planned on both rivers,
612 which, if built, will trap large amounts of sediment, strongly reducing the net export to
613 the deltas. Our results presented here thus establish an important pre-dam baseline of
614 sediment export by the Irrawaddy-Salween system.

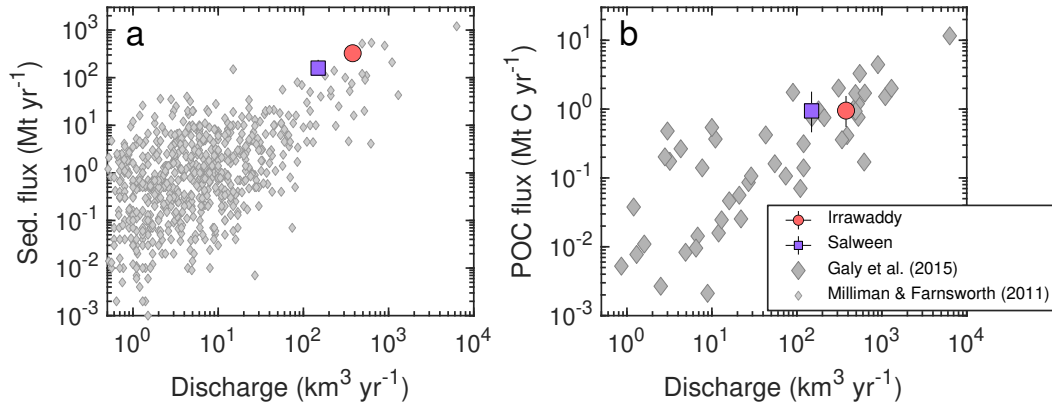


Figure 11. Comparison of the Irrawaddy and Salween (a) total sediment and (b) POC fluxes to other major global rivers.

6 Conclusions

In this contribution, we have presented a new semi-empirical hydrodynamic Rouse modeling approach to synoptically predict the two dimensional distribution suspended sediment concentration, physicochemical composition (grain size and organic carbon content), and flux in large, turbulent rivers with geomorphologically complex channels. We have applied this model to obtain spatially- and temporally-integrated estimates of the sediment composition and export flux of the Irrawaddy and Salween rivers in Southeast Asia. In comparison to the model, flux estimates derived from using simple means of evenly-spaced depth point samples can result in errors of up to 50%. This demonstrates that synoptic (i.e. spatially highly-resolved) sediment transport modeling is crucial for the accurate quantification of sediment composition and flux in large river channels, where wide sediment grain size distributions and variable hydraulic conditions result in complex sediment transport patterns.

Using the approach outlined above, we have calculated a total sediment flux of 485 (68% confidence interval of 364-654) Mt/yr and a particular carbon flux of 1.9 (1.0-3.3) Mt C/yr for the Irrawaddy-Salween system, accounting respectively for 2-3% and 0.8-1.2% of the total global riverine export to the ocean. These new estimates represent a \sim 20% and a 60-80% reduction of sediment and POC fluxes, respectively, compared to previously best estimates, which were partly based on 19th century data. While some of this difference may potentially be accounted for by actual changes in deforestation, land-use, and other anthropogenic pressures in the river basins, we suggest that most

636 of the difference is likely methodological, stemming from the use of a robust hydrody-
637 namic sediment transport model in the current study. We expect that the methods and
638 results described here, when combined with chemical and isotopic analyses of sediments
639 at these and other sites in the Irrawaddy and the Salween basins, will enable a deeper
640 understanding of the sediment provenance, erosion, and chemical weathering dynamics
641 in the region, with the ultimate aim of fully constraining the regional organic and inor-
642 ganic carbon cycle.

643 While the upstream sediment supply remains relatively constant, our calibrated
644 Rouse-model fits presented here allow the use of ADCP data to predict the spatial dis-
645 tribution of SSC and POC across each river channel in the future. In turn, our calibrated
646 SSC rating curves allow the prediction of total sediment flux with varying discharge. How-
647 ever, given that a number of large dams are planned on major tributaries and mainstems
648 of both rivers, sediment supply to their respective lower basins are expected to change,
649 if and once these dams are constructed. In this case, active, depth-sampling based mon-
650 itoring of sediment fluxes will be required to accurately quantify the changing sediment
651 flux and composition. In this case, the results of our current study provide an impor-
652 tant pre-dam baseline against which future changes can be evaluated.

653 **Acknowledgments**

654 All measurement and final model results are tabulated in the main text and in the Sup-
655 plementary Tables. Raw and processed ADCP data files and individual cross-section model
656 results are available on PANGAEA data repository (*author note: will be uploaded and*
657 *hyperlink included here upon acceptance*). Funding was provided by NERC Standard Grant
658 NE/P011659/1 to ETT, RJH, and MJB. We thank Si Thu, Charlie Eardley, Vivian Cum-
659 mings, Luke Bridgestock, Hazel Chapman, and staff of DWIR for help in the field. Tam-
660 sin O’Connell and Catherine Kneale (Dept. of Archaeology, U. of Cambridge) are thanked
661 for assisting with freeze drying. Olly Dawes and Laura Healy helped with sediment grain
662 size analyses at the University of Hull and the University of Cambridge, respectively.

663 **References**

664 Allison, M. a., Bianchi, T. S., McKee, B. a., & Sampere, T. P. (2007, 1). Carbon
665 burial on river-dominated continental shelves: Impact of historical changes in
666 sediment loading adjacent to the Mississippi River. *Geophysical Research*

- 667 *Letters*, 34, L01606. Retrieved from [http://doi.wiley.com/10.1029/](http://doi.wiley.com/10.1029/2006GL028362)
668 2006GL028362 doi: 10.1029/2006GL028362
- 669 Armijos, E., Crave, A., Espinoza, R., Fraizy, P., Santos, A. L., Sampaio, F., ... Fil-
670 izola, N. (2017). Measuring and modeling vertical gradients in suspended
671 sediments in the Solimões/Amazon River. *Hydrological Processes*, 31(3),
672 654–667. doi: 10.1002/hyp.11059
- 673 Bendixen, M., Best, J., Hackney, C., & Iversen, L. L. (2019, 7). Time is running out
674 for sand. *Nature*, 571(7763), 29–31. Retrieved from [http://www.nature.com/](http://www.nature.com/articles/d41586-019-02042-4)
675 [articles/d41586-019-02042-4](http://www.nature.com/articles/d41586-019-02042-4) doi: 10.1038/d41586-019-02042-4
- 676 Berner, R. A., & Kothavala, Z. (2001). Geocarb III: A revised model of atmospheric
677 CO₂ over phanerozoic time. *American Journal of Science*, 301(2), 182–204.
678 doi: 10.2475/ajs.301.2.182
- 679 Best, J. (2019, 1). Anthropogenic stresses on the world's big rivers. *Nature*
680 *Geoscience*, 12(1), 7–21. Retrieved from [http://dx.doi.org/10.1038/](http://dx.doi.org/10.1038/s41561-018-0262-x)
681 [s41561-018-0262-x](http://www.nature.com/articles/s41561-018-0262-x)
682 doi: 10.1038/s41561-018-0262-x
- 683 Bird, M., Robinson, R., Win Oo, N., Maung Aye, M., Lu, X., Higgitt, D., ...
684 Hoey, T. (2008, 8). A preliminary estimate of organic carbon trans-
685 port by the Ayeyarwady (Irrawaddy) and Thanlwin (Salween) Rivers of
686 Myanmar. *Quaternary International*, 186(1), 113–122. Retrieved from
687 <http://linkinghub.elsevier.com/retrieve/pii/S1040618207002170>
688 doi: 10.1016/j.quaint.2007.08.003
- 689 Bouchez, J., Gaillardet, J., France-Lanord, C., Maurice, L., & Dutra-Maia, P. (2011,
690 3). Grain size control of river suspended sediment geochemistry: Clues from
691 Amazon River depth profiles. *Geochemistry, Geophysics, Geosystems*, 12(3),
692 n/a-n/a. Retrieved from <http://doi.wiley.com/10.1029/2010GC003380>
693 doi: 10.1029/2010GC003380
- 694 Bouchez, J., Lupker, M., Gaillardet, J., France-Lanord, C., & Maurice, L. (2011,
695 11). How important is it to integrate riverine suspended sediment chem-
696 ical composition with depth? Clues from Amazon River depth-profiles.
697 *Geochimica et Cosmochimica Acta*, 75(22), 6955–6970. Retrieved from
698 <https://linkinghub.elsevier.com/retrieve/pii/S0016703711005047>
699 doi: 10.1016/j.gca.2011.08.038

- 700 Bouchez, J., Métivier, F., Lupker, M., Maurice, L., Perez, M., Gaillardet, J., &
701 France-Lanord, C. (2011). Prediction of depth-integrated fluxes of suspended
702 sediment in the Amazon River: Particle aggregation as a complicating factor.
703 *Hydrological Processes*, 25(5), 778–794. doi: 10.1002/hyp.7868
- 704 Chapman, H., Bickle, M., Thaw, S. H., & Thiam, H. N. (2015). Chemical fluxes
705 from time series sampling of the Irrawaddy and Salween Rivers, Myanmar.
706 *Chemical Geology*, 401, 15–27. Retrieved from [http://dx.doi.org/10.1016/](http://dx.doi.org/10.1016/j.chemgeo.2015.02.012)
707 [j.chemgeo.2015.02.012](http://dx.doi.org/10.1016/j.chemgeo.2015.02.012) doi: 10.1016/j.chemgeo.2015.02.012
- 708 Chen, C. J., Senarath, S. U., Dima-West, I. M., & Marcella, M. P. (2017). Eval-
709 uation and restructuring of gridded precipitation data over the Greater
710 Mekong Subregion. *International Journal of Climatology*, 37(1), 180–196.
711 doi: 10.1002/joc.4696
- 712 Darby, S. E., Hackney, C. R., Leyland, J., Kummu, M., Lauri, H., Parsons, D. R.,
713 ... Aalto, R. (2016). Fluvial sediment supply to a mega-delta reduced by
714 shifting tropical-cyclone activity. *Nature*, 539(7628), 276–279. Retrieved from
715 <http://dx.doi.org/10.1038/nature19809> doi: 10.1038/nature19809
- 716 D'Errico, J. (2018). *inpaint_nans*. MATLAB Central File Exchange. Re-
717 trieved from [https://www.mathworks.com/matlabcentral/fileexchange/](https://www.mathworks.com/matlabcentral/fileexchange/4551-inpaint_nans)
718 [4551-inpaint_nans](https://www.mathworks.com/matlabcentral/fileexchange/4551-inpaint_nans)
- 719 Dietrich, W. E. (1982). Settling velocity of natural particles. *Water Resources Re-*
720 *search*, 18(6), 1615–1626. doi: 10.1029/WR018i006p01615
- 721 Diplas, P., Dancey, C. L., Celik, A. O., Valyrakis, M., Greer, K., & Akar, T. (2008,
722 10). The Role of Impulse on the Initiation of Particle Movement Under
723 Turbulent Flow Conditions. *Science*, 322(5902), 717–720. Retrieved from
724 <http://www.sciencemag.org/cgi/doi/10.1126/science.1158954> doi:
725 10.1126/science.1158954
- 726 France-Lanord, C., & Derry, L. (1997). Organic carbon burial forcing of the carbon
727 cycle from Himalayan erosion. *Nature*, 390(November), 65–67. Retrieved from
728 [http://www.es.ucsc.edu/~rcoe/eart206/France-Lanord&Derry_Nature97](http://www.es.ucsc.edu/~rcoe/eart206/France-Lanord&Derry_Nature97.pdf)
729 [.pdf](http://www.es.ucsc.edu/~rcoe/eart206/France-Lanord&Derry_Nature97.pdf)
- 730 Furuichi, T., Win, Z., & Wasson, R. J. (2009, 5). Discharge and suspended
731 sediment transport in the Ayeyarwady River, Myanmar: centennial and
732 decadal changes. *Hydrological Processes*, 23(11), 1631–1641. Retrieved from

- 733 <http://doi.wiley.com/10.1002/hyp.7295> doi: 10.1002/hyp.7295
- 734 Gaillardet, J., Dupré, B., Louvat, P., & Allègre, C. (1999, 7). Global sil-
 735 icate weathering and CO₂ consumption rates deduced from the chem-
 736 istry of large rivers. *Chemical Geology*, 159(1-4), 3–30. Retrieved from
 737 <http://linkinghub.elsevier.com/retrieve/pii/S0009254199000315>
 738 doi: 10.1016/S0009-2541(99)00031-5
- 739 Galy, V., France-Lanord, C., Beyssac, O., Faure, P., Kudrass, H., & Palhol, F.
 740 (2007, 11). Efficient organic carbon burial in the Bengal fan sustained
 741 by the Himalayan erosional system. *Nature*, 450(7168), 407–10. Re-
 742 trieved from <http://www.ncbi.nlm.nih.gov/pubmed/18004382> doi:
 743 10.1038/nature06273
- 744 Galy, V., Peucker-Ehrenbrink, B., & Eglinton, T. (2015). Global carbon export from
 745 the terrestrial biosphere controlled by erosion. *Nature*, 521(7551), 204–207.
 746 Retrieved from <http://www.nature.com/doi/10.1038/nature14400>
 747 doi: 10.1038/nature14400
- 748 Godderis, Y., Roelandt, C., Schott, J., Pierret, M.-C., & Francois, L. M. (2009, 9).
 749 Towards an Integrated Model of Weathering, Climate, and Biospheric Pro-
 750 cesses. *Reviews in Mineralogy and Geochemistry*, 70(1), 411–434. Retrieved
 751 from <http://ring.geoscienceworld.org/cgi/doi/10.2138/rmg.2009.70.9>
 752 doi: 10.2138/rmg.2009.70.9
- 753 Gordon, R. (1880). *Report on the Irawadi River. Pt I-IV.* (Tech. Rep.). Rangoon:
 754 Secretariat.
- 755 Gray, J. R., & Gartner, J. W. (2009, 4). Technological advances in suspended-
 756 sediment surrogate monitoring. *Water Resources Research*, 45(4). Re-
 757 trieved from <http://doi.wiley.com/10.1029/2008WR007063> doi:
 758 10.1029/2008WR007063
- 759 Grill, G., Lehner, B., Thieme, M., Geenen, B., Tickner, D., Antonelli, F., ... Zarfl,
 760 C. (2019, 5). Mapping the world’s free-flowing rivers. *Nature*, 569(7755), 215–
 761 221. Retrieved from <http://www.nature.com/articles/s41586-019-1111-9>
 762 doi: 10.1038/s41586-019-1111-9
- 763 Guo, L., & He, Q. (2011). Freshwater flocculation of suspended sediments in the
 764 Yangtze River, China. *Ocean Dynamics*, 61(2-3), 371–386. doi: 10.1007/s10236
 765 -011-0391-x

- 766 Hackney, C. R., Darby, S. E., Parsons, D. R., Leyland, J., Best, J. L., Aalto, R., ...
767 Houseago, R. C. (2020, 1). River bank instability from unsustainable sand
768 mining in the lower Mekong River. *Nature Sustainability*. Retrieved from
769 <http://dx.doi.org/10.1038/s41893-019-0455-3>[http://www.nature.com/](http://www.nature.com/articles/s41893-019-0455-3)
770 [articles/s41893-019-0455-3](http://www.nature.com/articles/s41893-019-0455-3) doi: 10.1038/s41893-019-0455-3
- 771 Hilton, R. G., Galy, A., Hovius, N., Chen, M.-C., Horng, M.-J., & Chen, H. (2008).
772 Tropical-cyclone-driven erosion of the terrestrial biosphere from mountains.
773 *Nature Geoscience*, 1, 759–762. doi: 10.1038/ngeo333
- 774 Hilton, R. G., Galy, V., Gaillardet, J., Dellinger, M., Bryant, C., O'Regan, M., ...
775 Calmels, D. (2015). Erosion of organic carbon in the Arctic as a geological
776 carbon dioxide sink. *Nature*, 524(7563), 84–87. doi: 10.1038/nature14653
- 777 Horan, K., Hilton, R., Dellinger, M., Tipper, E., Galy, V., Calmels, D., ... Burton,
778 K. (2019). Carbon dioxide emissions by rock organic carbon oxidation and
779 the net geochemical carbon budget of the Mackenzie River Basin. *American*
780 *Journal of Science*, 319, 473–499. doi: 10.2475/06.2019.02
- 781 Jordan, P. (1965). *Fluvial sediment of the mississippi river at St. Louis, Mis-*
782 *souri* (Tech. Rep.). United States Army. Corps of Engineers. Retrieved from
783 <http://pubs.usgs.gov/wsp/1802/report.pdf>
- 784 Khin Zaw, Win Swe, Barber, A. J., Crow, M. J., & Yin Yin Nwe. (2017, 11). In-
785 troduction to the geology of Myanmar. *Geological Society, London, Memoirs*,
786 48(1), 1–17. Retrieved from [http://mem.lyellcollection.org/lookup/doi/](http://mem.lyellcollection.org/lookup/doi/10.1144/M45.01)
787 [10.1144/M45.01](http://mem.lyellcollection.org/lookup/doi/10.1144/M45.01)[http://mem.lyellcollection.org/lookup/doi/10.1144/](http://mem.lyellcollection.org/lookup/doi/10.1144/M48.1)
788 [M48.1](http://mem.lyellcollection.org/lookup/doi/10.1144/M48.1) doi: 10.1144/M48.1
- 789 Kirchherr, J., J. Charles, K., & Walton, M. J. (2017). The interplay of activists
790 and dam developers: the case of Myanmar's mega-dams. *International Jour-*
791 *nal of Water Resources Development*, 33(1), 111–131. Retrieved from [http://](http://dx.doi.org/10.1080/07900627.2016.1179176)
792 dx.doi.org/10.1080/07900627.2016.1179176 doi: 10.1080/07900627.2016
793 .1179176
- 794 Komada, T., Anderson, M. R., & Dorfmeier, C. L. (2008). Carbonate removal from
795 coastal sediments for the determination of organic carbon and its isotopic sig-
796 natures, $\delta^{13}\text{C}$ and $\Delta^{14}\text{C}$: comparison of fumigation and direct acidification
797 by hydrochloric acid. *Limnology and Oceanography: Methods*, 6(6), 254–262.
798 doi: 10.4319/lom.2008.6.254

- 799 Kondolf, G. M., Schmitt, R. J., Carling, P., Darby, S., Arias, M., Bizzi, S., . . . Wild,
800 T. (2018). Changing sediment budget of the Mekong: Cumulative threats
801 and management strategies for a large river basin. *Science of the Total*
802 *Environment*, *625*, 114–134. Retrieved from [https://doi.org/10.1016/](https://doi.org/10.1016/j.scitotenv.2017.11.361)
803 [j.scitotenv.2017.11.361](https://doi.org/10.1016/j.scitotenv.2017.11.361) doi: 10.1016/j.scitotenv.2017.11.361
- 804 Kostaschuk, R., Best, J., Villard, P., Peakall, J., & Franklin, M. (2005). Measuring
805 flow velocity and sediment transport with an acoustic Doppler current profiler.
806 *Geomorphology*, *68*(1-2), 25–37. doi: 10.1016/j.geomorph.2004.07.012
- 807 Latosinski, F. G., Szupiany, R. N., García, C. M., Guerrero, M., & Amsler,
808 M. L. (2014). Estimation of Concentration and Load of Suspended
809 Bed Sediment in a Large River by Means of Acoustic Doppler Technol-
810 ogy. *Journal of Hydraulic Engineering*, *140*(7), 04014023. Retrieved from
811 <http://ascelibrary.org/doi/10.1061/%28ASCE%29HY.1943-7900.0000859>
812 doi: 10.1061/(ASCE)HY.1943-7900.0000859
- 813 Lazarus, K., Cardinale, P., Corbett, M., Lin, N. S., & Noeske, T. (2019). *Strate-*
814 *gic Environmental Assessment of the Hydropower Sector in Myanmar :*
815 *Baseline Assessment Report* (Tech. Rep.). Washington, D.C: World Bank
816 Group. Retrieved from [http://documents.worldbank.org/curated/en/](http://documents.worldbank.org/curated/en/126001548867293771/Baseline-Assessment-Report-Introduction)
817 [126001548867293771/Baseline-Assessment-Report-Introduction](http://documents.worldbank.org/curated/en/126001548867293771/Baseline-Assessment-Report-Introduction)
- 818 Licht, A., France-Lanord, C., Reisberg, L., Fontaine, C., Soe, A. N., & Jaeger,
819 J.-J. (2013). A palaeo Tibet–Myanmar connection? Reconstructing the
820 Late Eocene drainage system of central Myanmar using a multi-proxy ap-
821 proach. *Journal of the Geological Society*, *170*(6), 929–939. Retrieved from
822 <http://jgs.lyellcollection.org/lookup/doi/10.1144/jgs2012-126> doi:
823 10.1144/jgs2012-126
- 824 Lupker, M., France-Lanord, C., Lavé, J., Bouchez, J., Galy, V., Métivier, F., . . .
825 Mugnier, J.-L. (2011, 11). A Rouse-based method to integrate the chemi-
826 cal composition of river sediments: Application to the Ganga basin. *Jour-*
827 *nal of Geophysical Research*, *116*(F4), F04012. Retrieved from [http://](http://doi.wiley.com/10.1029/2010JF001947)
828 doi.wiley.com/10.1029/2010JF001947 doi: 10.1029/2010JF001947
- 829 Mackenzie, F. T., & Garrels, R. M. (1966, 9). Chemical mass balance between
830 rivers and oceans. *American Journal of Science*, *264*(7), 507–525. Retrieved
831 from <http://www.ajsonline.org/cgi/doi/10.2475/ajs.264.7.507> doi:

- 832 10.2475/ajs.264.7.507
- 833 Maher, K., & Chamberlain, C. P. (2014, 3). Hydrologic regulation of chemi-
 834 cal weathering and the geologic carbon cycle. *Science*, *343*(6178), 1502–
 835 4. Retrieved from [http://science.sciencemag.org/content/343/6178/](http://science.sciencemag.org/content/343/6178/1502.1long)
 836 1502.1long doi: 10.1126/science.1250770
- 837 Meade, R. H. (1994). Suspended sediments of the modern Amazon and Orinoco
 838 rivers. *Quaternary International*, *21*(C), 29–39. doi: 10.1016/1040-6182(94)
 839 90019-1
- 840 Meade, R. H., & Stevens, H. H. (1990). Strategies and equipment for sampling
 841 suspended sediment and associated toxic chemicals in large rivers - With
 842 emphasis on the Mississippi river. *Science of the Total Environment*, *The*,
 843 *97-98*(C), 125–135. doi: 10.1016/0048-9697(90)90235-M
- 844 Meybeck, M. (1987). *Global Chemical Weathering of Surficial Rocks Estimated From*
 845 *River Dissolved Loads*. (Vol. 287) (No. 5). doi: 10.2475/ajs.287.5.401
- 846 Meybeck, M., & Ragu, A. (1997). *River discharges to the oceans: an assessment of*
 847 *suspended solids, major ions and nutrients* (Tech. Rep.). UNEP.
- 848 Miller, M., McCave, I. N., & Komar, P. (1977). Threshold of sediment motion under
 849 unidirectional currents. *Sedimentology*, 507–527. doi: 10.1111/j.1365-3091.1977
 850 .tb00136.x
- 851 Milliman, J. D., & Farnsworth, K. L. (2011). *River Discharge to the Coastal*
 852 *Ocean*. Cambridge: Cambridge University Press. Retrieved from
 853 <http://ebooks.cambridge.org/ref/id/CB09780511781247> doi: 10.1017/
 854 CBO9780511781247
- 855 Mitchell, A., Chung, S. L., Oo, T., Lin, T. H., & Hung, C. H. (2012). Zircon
 856 U-Pb ages in Myanmar: Magmatic-metamorphic events and the closure
 857 of a neo-Tethys ocean? *Journal of Asian Earth Sciences*, *56*, 1–23. Re-
 858 trieved from <http://dx.doi.org/10.1016/j.jseaes.2012.04.019> doi:
 859 10.1016/j.jseaes.2012.04.019
- 860 Morin, G. P., Lavé, J., France-Lanord, C., Rigaudier, T., Gajurel, A. P., & Sinha, R.
 861 (2018). Annual Sediment Transport Dynamics in the Narayani Basin, Central
 862 Nepal: Assessing the Impacts of Erosion Processes in the Annual Sediment
 863 Budget. *Journal of Geophysical Research: Earth Surface*, *123*(10), 2341–2376.
 864 doi: 10.1029/2017JF004460

- 865 Murray Hicks, D., & Gomez, B. (2016, 4). Sediment transport. In G. Kon-
 866 dolf & H. Piégay (Eds.), *Tools in fluvial geomorphology* (2nd ed., pp. 324–
 867 356). Chichester, UK: Wiley. Retrieved from [https://doi.org/10.1002/](https://doi.org/10.1002/9781118648551.ch15)
 868 [9781118648551.ch15](https://onlinelibrary.wiley.com/doi/abs/10.1002/9781118648551.ch15)[https://onlinelibrary.wiley.com/doi/abs/10.1002/](https://onlinelibrary.wiley.com/doi/abs/10.1002/9781118648551.ch15)
 869 [9781118648551.ch15](https://onlinelibrary.wiley.com/doi/abs/10.1002/9781118648551.ch15) doi: 10.1002/9781118648551.ch15
- 870 Muste, M., Yu, K., Fujita, I., & Ettema, R. (2005). Two-phase versus mixed-flow
 871 perspective on suspended sediment transport in turbulent channel flows. *Water*
 872 *Resources Research*, *41*(10). doi: 10.1029/2004WR003595
- 873 Najman, Y., Sobel, E. R., Millar, I., Stockli, D. F., Govin, G., Lisker, F., ...
 874 Kahn, A. (2020, 1). The exhumation of the Indo-Burman Ranges, Myan-
 875 mar. *Earth and Planetary Science Letters*, *530*, 115948. Retrieved from
 876 <https://linkinghub.elsevier.com/retrieve/pii/S0012821X19306405>
 877 doi: 10.1016/j.epsl.2019.115948
- 878 Pal, D., & Ghoshal, K. (2016). Effect of particle concentration on sediment and
 879 turbulent diffusion coefficients in open-channel turbulent flow. *Environmental*
 880 *Earth Sciences*, *75*(18), 1–11. doi: 10.1007/s12665-016-6045-z
- 881 Parsons, D. R., Jackson, P. R., Czuba, J. A., Engel, F. L., Rhoads, B. L., Oberg,
 882 K. A., ... Riley, J. D. (2013). Velocity Mapping Toolbox (VMT): A processing
 883 and visualization suite for moving-vessel ADCP measurements. *Earth Surface*
 884 *Processes and Landforms*, *38*(11), 1244–1260. doi: 10.1002/esp.3367
- 885 Robinson, R., Bird, M., Oo, N. W., Hoey, T., Aye, M. M., Higgitt, D., ... Win,
 886 S. L. (2007, 11). The Irrawaddy River Sediment Flux to the Indian Ocean:
 887 The Original Nineteenth-Century Data Revisited. *The Journal of Geology*,
 888 *115*(6), 629–640. Retrieved from [https://www.jstor.org/stable/10.1086/](https://www.jstor.org/stable/10.1086/521607)
 889 [521607](https://www.journals.uchicago.edu/doi/10.1086/521607)<https://www.journals.uchicago.edu/doi/10.1086/521607> doi:
 890 10.1086/521607
- 891 Rouse, H. (1950). Fundamental principles of flow. *Engineering hydraulics*, 1–135.
- 892 Santini, W., Camenen, B., Le Coz, J., Vauchel, P., Guyot, J.-L., Lavado, W., ...
 893 Martinez, J.-M. (2019). An index concentration method for suspended load
 894 monitoring in large rivers of the Amazonian foreland. *Earth Surface Dynamics*,
 895 1–36. doi: 10.5194/esurf-2018-93
- 896 Searle, M. P., Noble, S. R., Cottle, J. M., Waters, D. J., Mitchell, A. H., Hlaing, T.,
 897 & Horstwood, M. S. (2007). Tectonic evolution of the Mogok metamorphic

- 898 belt, Burma (Myanmar) constrained by U-Th-Pb dating of metamorphic and
 899 magmatic rocks. *Tectonics*, *26*(3). doi: 10.1029/2006TC002083
- 900 Sein, K. K., Chidthaisong, A., & Oo, K. L. (2018). Observed Trends and Changes in
 901 Temperature and Precipitation Extreme Indices over Myanmar. *Atmosphere*,
 902 *9*(12), 477. Retrieved from <https://doi.org/10.3390/atmos9120477> doi: 10
 903 .3390/atmos9120477
- 904 Syvitski, J. P., & Kettner, A. (2011). Sediment flux and the anthropocene. *Philo-*
 905 *sophical Transactions of the Royal Society A: Mathematical, Physical and*
 906 *Engineering Sciences*, *369*(1938), 957–975. doi: 10.1098/rsta.2010.0329
- 907 Syvitski, J. P., Vörösmarty, C. J., Kettner, A. J., & Green, P. (2005). Impact of
 908 humans on the flux of terrestrial sediment to the global coastal ocean. *Science*,
 909 *308*(5720), 376–380. doi: 10.1126/science.1109454
- 910 Szupiany, R. N., Amsler, M. L., Best, J. L., & Parsons, D. R. (2007). Compar-
 911 ison of Fixed- and Moving-Vessel Flow Measurements with an aDp in a
 912 Large River. *Journal of Hydraulic Engineering*, *133*(12), 1299–1309. doi:
 913 10.1061/(asce)0733-9429(2007)133:12(1299)
- 914 Szupiany, R. N., Lopez Weibel, C., Guerrero, M., Latosinski, F., Wood, M.,
 915 Dominguez Ruben, L., & Oberg, K. (2019, 5). Estimating sand con-
 916 centrations using ADCP-based acoustic inversion in a large fluvial sys-
 917 tem characterized by bi-modal suspended-sediment distributions. *Earth*
 918 *Surface Processes and Landforms*, *44*(6), 1295–1308. Retrieved from
 919 <https://onlinelibrary.wiley.com/doi/abs/10.1002/esp.4572> doi:
 920 10.1002/esp.4572
- 921 Thorne, P. D., & Hanes, D. M. (2002, 3). A review of acoustic measurement of
 922 small-scale sediment processes. *Continental Shelf Research*, *22*(4), 603–
 923 632. Retrieved from [https://linkinghub.elsevier.com/retrieve/pii/
 924 S0278434301001017](https://linkinghub.elsevier.com/retrieve/pii/S0278434301001017) doi: 10.1016/S0278-4343(01)00101-7
- 925 van Rijn, L. C., Walstra, D.-J. R., & van Ormondt, M. (2007). Unified View of Sed-
 926 iment Transport by Currents and Waves. IV: Application of Morphodynamic
 927 Model. *Journal of Hydraulic Engineering*, *133*(7), 776–793. Retrieved from
 928 [http://ascelibrary.org/doi/10.1061/%28ASCE%290733-9429%282007%
 929 29133%3A7%28776%29](http://ascelibrary.org/doi/10.1061/%28ASCE%290733-9429%282007%29133%3A7%28776%29) doi: 10.1061/(ASCE)0733-9429(2007)133:7(776)
- 930 Viers, J., Oliva, P., Dandurand, J. L., Dupr??, B., & Gaillardet, J. (2013). Chemical

- 931 Weathering Rates, CO₂ Consumption, and Control Parameters Deduced from
 932 the Chemical Composition of Rivers. In *Treatise on geochemistry: Second*
 933 *edition* (Vol. 7, pp. 175–194). doi: 10.1016/B978-0-08-095975-7.00506-4
- 934 Wang, H., Yang, Z., Saito, Y., Liu, J. P., Sun, X., & Wang, Y. (2007). Stepwise
 935 decreases of the Huanghe (Yellow River) sediment load (1950-2005): Impacts
 936 of climate change and human activities. *Global and Planetary Change*, *57*(3-4),
 937 331–354. doi: 10.1016/j.gloplacha.2007.01.003
- 938 West, A., Galy, A., & Bickle, M. (2005, 6). Tectonic and climatic controls on silicate
 939 weathering. *Earth and Planetary Science Letters*, *235*(1-2), 211–228. Retrieved
 940 from <http://linkinghub.elsevier.com/retrieve/pii/S0012821X05002116>
 941 doi: 10.1016/j.epsl.2005.03.020
- 942 Westerweel, J., Roperch, P., Licht, A., Dupont-Nivet, G., Win, Z., Poblete, F.,
 943 ... Aung, D. W. (2019). Burma Terrane part of the Trans-Tethyan arc
 944 during collision with India according to palaeomagnetic data. *Nature Geo-*
 945 *science*, *12*(October). Retrieved from [http://dx.doi.org/10.1038/](http://dx.doi.org/10.1038/s41561-019-0443-2)
 946 [s41561-019-0443-2](http://dx.doi.org/10.1038/s41561-019-0443-2) doi: 10.1038/s41561-019-0443-2
- 947 Wilkinson, B. H., & McElroy, B. J. (2007). The impact of humans on continen-
 948 tal erosion and sedimentation. *Bulletin of the Geological Society of America*,
 949 *119*(1-2), 140–156. doi: 10.1130/B25899.1
- 950 Xiqing, C., Qiaoju, Z., & Erfeng, Z. (2006). In-channel sand extraction from the
 951 mid-lower Yangtze channels and its management: Problems and challenges.
 952 *Journal of Environmental Planning and Management*, *49*(2), 309–320. doi:
 953 10.1080/09640560500508247
- 954 Yamazaki, D., Ikeshima, D., Sosa, J., Bates, P. D., Allen, G., & Pavelsky, T. (2019).
 955 MERIT Hydro: A high-resolution global hydrography map based on latest
 956 topography datasets. *Water Resources Research*, 2019WR024873. Retrieved
 957 from <https://onlinelibrary.wiley.com/doi/abs/10.1029/2019WR024873>
 958 doi: 10.1029/2019WR024873
- 959 Yorke, T. H., & Oberg, K. A. (2002). Measuring river velocity and discharge with
 960 acoustic Doppler profilers. *Flow Measurement and Instrumentation*, *13*(5-6),
 961 191–195. doi: 10.1016/S0955-5986(02)00051-1
- 962 Zhang, J., Xiao, W., Windley, B. F., Wakabayashi, J., Cai, F., Sein, K., ... Naing,
 963 S. (2018). *Multiple alternating forearc- and backarc-ward migration of mag-*

964 *matism in the Indo-Myanmar Orogenic Belt since the Jurassic: Documenta-*
965 *tion of the orogenic architecture of eastern Neotethys in SE Asia* (Vol. 185)
966 (No. January). Elsevier. Retrieved from [https://doi.org/10.1016/](https://doi.org/10.1016/j.earscirev.2018.07.009)
967 [j.earscirev.2018.07.009](https://doi.org/10.1016/j.earscirev.2018.07.009) doi: 10.1016/j.earscirev.2018.07.009